Parameterization of cloud droplet formation in global climate models

ATHANASIOS NENES [1]and JOHN H. SEINFELD

Department of Chemical Engineering, Mail Code 210-41, California Institute of Technology, Pasadena, California

Short title:

[1]Currently at Schools of Earth and Atmospheric Sciences and Chemical Engineering, Georgia Institute of Technology, Atlanta, Georgia

Abstract. An aerosol activation parameterization has been developed, based on a generalized representation of aerosol size and composition within the framework of an ascending adiabatic parcel; this allows for parameterizing the activation of chemically complex aerosol with arbitrary size distribution and mixing state. The new parameterization introduces the concept of "population splitting", in which the CCN that form droplets are treated as two separate populations: those which have a size close to their critical diameter, and those that do not. Explicit consideration of kinetic limitations on droplet growth is introduced. Our treatment of the activation process unravels much of its complexity. As a result of this, a substantial number of conditions of droplet formation can be treated completely free of empirical information or correlations; there are, however, some conditions of droplet activation for which an empirically derived correlation is utilized. Predictions of the parameterization are compared against extensive cloud parcel model simulations, for a variety of aerosol activation conditions that cover a wide range of chemical variability and CCN concentrations. The parameterization tracks the parcel model simulations closely and robustly. The parameterization presented here is intended to allow for a comprehensive assessment of the aerosol indirect effect in GCMs.

1. Introduction

The most uncertain of all climate forcings is the aerosol indirect effect [*Intergovernmental Panel on Climate Change (IPCC)*, 2001]. There are two reasons for this. The first originates from the wide range of length scales involved in cloud-aerosol interactions: from hundreds of kilometers (that of the largest cloud systems) down to tens of meters (that of individual updrafts responsible for production of new drops). Sizes of typical General Circulation Model (GCM) grid cells range from $4^o \times 5^o$ to $2^o \times 2^o$. Such grid sizes can resolve only the largest cloud systems. To estimate how aerosol perturbations affect cloud properties from first principles, one needs to explicitly resolve processes that take place down to the smallest scales of new droplet formation. Cloud-resolving large eddy simulations can potentially address these smaller length scales, but the computational burden associated with such simulations prohibits their use in climate models. The second reason lies in the sheer complexity of aerosol-cloud interactions themselves.

The first attempts to relate cloud properties to aerosols in GCMs (e.g. *Boucher and Lohmann* [1995]; *Kiehl* [1999]) empirically linked cloud droplet number concentration to a property available in a global aerosol model, such as total aerosol sulfate mass (e.g. *Boucher and Lohmann* [1995]), or total aerosol number (e.g. *Gultepe and Isaac* [1996]). The empirical relationship itself is subject to substantial uncertainty; aerosol-cloud interactions are highly complex and cannot be represented by a simple correlation based on a single aerosol property. This is illustrated by the *Kiehl et al.* [2000] study,

in which several different empirical relationships yield estimates of the global annual average indirect forcing ranging between -0.40 W m^{-2} and -1.78 W m^{-2}. To address the deficiencies of purely empirical correlations, first-principle approaches to predicting cloud droplet number have emerged (e.g., *Ghan et al.* [1997]; *Lohmann et al.* [1999]).

Calculation of cloud droplet number from first principles entails setting up a cloud droplet number balance in each GCM grid cell,

$$\frac{dN_d}{dt} = Q_{activation} - Q_{evaporation} - Q_{collision} + Q_{advection} + ... \quad (1)$$

where N_d is the droplet number concentration, $Q_{activation}$ is the droplet source from droplet activation, $Q_{evaporation}$ is the loss from droplet evaporation, $Q_{collision}$ is the loss from collision-coalescence processes, and $Q_{advection}$ is the net source of droplets advected from adjacent grid cells (other processes can be present, particularly if the cloud contains ice or is precipitating). Cloud droplet activation is a key process for the indirect effect, since it is the direct microphysical aerosol-cloud link. Explicitly resolving each of these processes from first principles necessitate resolution on scales of tens of meters, since this is the smallest scale for which aerosol droplet activation, and hence cloud formation, can take place. Such resolutions are far beyond anything computationally feasible for GCMs. As a consequence, a prognostic GCM estimate of the aerosol indirect effect must rely on parameterizations of all such sub-grid processes. Implementation of explicit aerosol activation within a GCM presupposes that the dynamics of cloud formation (particularly the probability distribution of updraft velocity

or cooling rate below cloud), and the aerosol characteristics below cloud are known. Such dynamical information is not readily available from a GCM, so it must be obtained from a parameterization. The basic theory of aerosol activation is well established, and many numerical models describing it have appeared in the literature (e.g., *Jensen and Charlson* [1984]; *Flossmann et al.* [1985]; *Pruppacher and Klett* [1997]; *Seinfeld and Pandis* [1998]; *Nenes et al.* [2001]); inclusion of numerical activation models is in itself computationally challenging, so the activation process needs to be parameterized. Parameterization of the subgrid cloud dynamics is not addressed in the current study.

In parameterizations of aerosol activation that have appeared in the literature over the years, treatments of the aerosol size distribution and activation process differ. The first parameterization appeared four decades ago (e.g. *Twomey* [1959]; *Squires and Twomey* [1960]). Although providing elegant solutions and simple expressions for the number of nucleated droplets, these approaches rely on both simple aerosol size distributions (power law) and idealized expressions for droplet condensation rate. As a result, systematic errors arise in their predictions, such as prediction of droplet number that exceeds the total condensation nuclei. Other subsequent approaches have adopted a functional relationship between number of CCN that activate at a given supersaturation level (otherwise known as the "CCN spectrum"). *Feingold and Heymsfield* [1992] adopted a power law to describe the CCN spectrum, although their approach can be extended to any functional form. *Cohard et al.* [1998, 2000] in their treatment assumed a generalized sigmoidal function. The abstraction and detachment from assumptions regarding size distribution and chemical homogeneity

theoretically can allow any size distribution to be described through the generalized CCN spectrum. Other parameterizations have used log-normal representations of aerosol size distributions, and used Köhler theory to compute the CCN spectrum (e.g., [*Ghan et al.*, 1993, 1995; *Abdul-Razzak et al.*, 1998; *Abdul-Razzak and Ghan*, 2000]). *Abdul-Razzak and Ghan* [2002] propose an algorithm for use of their multiple log-normal population parameterization [*Abdul-Razzak and Ghan*, 2000] in sectional aerosol models. Their approach is to use an empirically prescribed value of geometric dispersion, and treat each section as a separate mode. *Chuang and Penner* [1995] parameterized sulfate transfer to and production in preexisting particles by condensation of gas-phase sulfuric acid and aqueous oxidation of sulfur dioxide. The most sophisticated current aerosol activation parameterizations still rely principally on empirical information obtained from detailed numerical parcel simulations. To compute the number of activated droplets, *Feingold and Heymsfield* [1992] compute the cloud maximum supersaturation from a nonlinear equation, which contains a parameter evaluated through multivariate regression of numerical adiabatic parcel calculations. *Abdul-Razzak et al.* [1998] and *Abdul-Razzak and Ghan* [2000] calculate the maximum parcel supersaturation explicitly, by using a correlation derived from regression of numerical parcel calculations. *Khvorostyanov and Curry* [1999] assume a power law aerosol size distribution to develop an analytical expression linking CCN number concentration to parameters that are related to aerosol growth under subsaturated conditions.

To summarize, previous aerosol activation parameterizations assume one (or more) of the following: i) specified aerosol size distributions (power law, log-normal), or

prescribed activation spectrum; ii) uniform chemical composition over particle size composed of only a completely soluble and insoluble fraction; iii) a single aerosol population (that is, an internally mixed aerosol); and iv) instantaneous activation of CCN (absence of kinetic effects). Any of these assumptions, under certain conditions, may not be satisfied, so application of the parameterization may lead to bias. The aerosol may be chemically complex, the composition of which can vary considerably with size and may be externally mixed. Certain aerosol chemical components can alter the activation behavior, in a manner which is not easily introduced in parameterizations. For example, the presence of surface active species, i.e., those that tend to lower the droplet surface tension, facilitate the activation of CCN [*Facchini et al.*, 1999]. The amount of surface tension depression depends on the concentration of the dissolved organic (e.g. *Shulman et al.* [1996]; *Charlson et al.* [2001]); since the concentration of dissolved species at the point of activation varies considerably with CCN dry size, one cannot assume a uniform or average change in surface tension throughout the CCN population. The resulting modified Köhler equation for such CCN cannot be solved explicitly for their critical supersaturation, s_c. As most extant parameterizations rely on an explicit link between s_c and dry CCN diameter, it is difficult to incorporate the implicit link surface-active species impose between s_c (or D_c) and the CCN dry size. Similar difficulties arise from the presence of slightly soluble species [*Laaksonen et al.*, 1998], which can also exhibit surface-active behavior. Such "chemical" effects cannot be neglected, as they can potentially constitute a large component of the aerosol indirect effect [*Charlson et al.*, 2001; *Nenes et al.*, 2002a]. Also, with the emergence of global

aerosol models that allow completely general distributions of both size and composition [*Adams and Seinfeld*, 2002], the stipulation of a prescribed distribution may be overly constraining. For example, the constraint that the aerosol has to follow a log-normal distribution has been shown to lead to discrepancies in droplet number when applied in a 1-D climate model [*Zhang et al.*, 2002]. The generalized CCN spectrum approach of *Cohard et al.* [1998, 2000], when used in conjunction with a GCM simulation of global aerosols, necessitates an undesirable on-line curve-fitting procedure.

Although utilizing empirical information can be a powerful tool, it is desirable, for sake of generality and robustness, to minimize the amount of such information contained within a parameterization. It is not clear when a parameterization, which is based on empirical fits, will exhibit biases in the prediction. For example, *Abdul-Razzak and Ghan* [2002] show that the sectional version of their activation parameterization follows a full numerical activation model for high updraft velocities, but the performance deteriorates as the updraft velocity decreases. For log-normal aerosol, the parcel model results are generally reproduced well when 10-90 % of the aerosol becomes activated [*Abdul-Razzak and Ghan*, 2000; *Abdul-Razzak et al.*, 1998].

The present work develops a new aerosol activation parameterization, intended for use in GCMs, which is based on a generalized representation of aerosol size and composition within the framework of an adiabatic cloud parcel. Explicit treatment of mass transfer (kinetic) limitations in droplet growth is included. We focus on minimizing the amount of empirical information included within the parameterization. In the sections that follow, we present the derivation of the activation parameterization and

then outline its use. We compare the new parameterization with that of *Abdul-Razzak and Ghan* [2000]; the two are compared to the predictions of a cloud parcel model with detailed growth kinetics for a variety of cloud condensation nucleus (CCN) activation conditions.

2. Definition of size distributions

Although any size distribution (such as a power law or lognormal) can be used in the new parameterization, we select a sectional representation to allow the most general possible representation of aerosol size and composition. In this representation, we divide the aerosol into an arbitrary number of size sections, each of which has its own chemical composition. Each section m is characterized by its lower and upper diameters, $D_{p,m-1}$ and $D_{p,m}$, and the total number concentration of particles in the section, N_m (Figure 1a). The aerosol chemical composition within each section is assumed to be uniform, and independent of those in other sections. A linear profile (which is a common assumption for sectional implementations of aerosol microphysics) of aerosol number concentration across a section is assumed. With these assumptions, the size distribution, $n^d(D_p) = dN/dD_p$, over $D_{p,m-1} \leq D_p < D_{p,m}$, is given by,

$$n^d(D_p) = \frac{dN}{dD_p} = \frac{N_m}{D_{p,m} - D_{p,m-1}} \tag{2}$$

and the cumulative size distribution (total number of particles with diameter smaller than D_p), $F^d(D_p)$, is given by,

$$F^d\left(D_p\right) = \int_0^{D_p} n^d\left(D'_p\right) dD'_p = \sum_{j=1}^{m-1} N_j + N_m \left(\frac{D_p - D_{p,m-1}}{D_{p,m} - D_{p,m-1}}\right) \tag{3}$$

where m is the section that contains D_p.

The above treatment assumes a single aerosol population. Multiple aerosol populations can exist (externally mixed aerosol); in this case, a separate size distribution, $n_k^d\left(D_p\right)$, is defined for each population, k. Then the cumulative size distribution is given by summing over all the populations,

$$F^d\left(D_p\right) = \sum_{l=1}^{k} \int_0^{D_p} n_l^d\left(D'_p\right) dD'_p = \sum_{l=1}^{k} \left\{ \sum_{j=1}^{m(l)-1} N_{j,l} + N_{m(l),l} \left(\frac{D_p - D^l_{p,m(l)-1}}{D^l_{p,m(l)} - D^l_{p,m(l)-1}}\right) \right\} \tag{4}$$

where $D^l_{p,m(l)-1}$, $D^l_{p,m(l)}$ are the boundaries of section i that contain D_p and population l. $m(l)$ is used to indicate that each population l has its own section boundaries.

3. Definition of CCN spectrum

After the size distributions are defined for each of the aerosol populations, $n^d\left(D_p\right)$ is then mapped to supersaturation space (Figure 1b), and the critical supersaturation distribution, $n^s\left(s\right)$, is obtained,

$$n^s\left(s\right) = \frac{dN}{ds} = \frac{N_i}{s_{c,i} - s_{c,i-1}}, \quad s_{c,i-1} \le s < s_{c,i} \tag{5}$$

where $s_{c,i-1}$ and $s_{c,i}$ are the critical supersaturations corresponding to the boundaries of section i. For simplicity, we assumed that $n^s(s)$ is piecewise linear. We change the index used for representing a section from m to i, to reflect the change in the ordering of the sections as they are mapped onto (monotonically increasing) supersaturation space.

The critical supersaturation corresponding to the section boundaries can be calculated using Köhler theory (i.e. the critical supersaturation corresponding to the diameter of each section boundary is calculated). We will not present a procedure for calculating the critical supersaturation of the sectional boundaries, as it is a standard procedure that can be found throughout the literature (e.g., *Seinfeld and Pandis* [1998]). We would like to note however, that we do not need an explicit link between aerosol dry size and critical supersaturation, a restraint which is necessary in most parameterizations. Relaxing this restraint allows for addressing the activation of highly complex activation curves, such as that seen for slightly soluble and surface active compounds [*Shulman et al.*, 1996].

The sectional representation of the CCN spectrum (total number of particles with critical supersaturation smaller than s), $F^s(s)$, is given by,

$$F^s(s) = \int_0^s n^s(s')\,ds' = \sum_{j=1}^{i-1} N_j + N_i \left(\frac{s - s_{c,i-1}}{s_{c,i} - s_{c,i-1}} \right) \tag{6}$$

where i is the section that contains s, and $s_{c,0} = 0$.

When k populations exist, the CCN spectrum is obtained by summing over all the aerosol populations,

$$F^s(s) = \sum_{l=1}^{k} \int_0^s n_l^s(s')\,ds' = \sum_{l=1}^{k} \left\{ \sum_{j=1}^{i(l)-1} N_{j,l} + N_{i(l),l} \left(\frac{s - s^l_{c,i(l)-1}}{s^l_{c,i(l)} - s^l_{c,i(l)-1}} \right) \right\} \tag{7}$$

where $s^l_{c,i(l)-1}$, $s^l_{c,i(l)}$ are the critical supersaturations for the boundaries of section i and population l that bound s. $i(l)$ is used to indicate that each population l has its own

section boundaries.

Equation 7 represents the CCN spectrum of the aerosol; once the maximum parcel supersaturation, s_{max}, is known, the number of CCN that will activate into drops, N_d, is given by,

$$N_d = F^s(s_{max}) \tag{8}$$

4. Formulation of the Aerosol Activation Parameterization

The aerosol activation parameterization is developed in two steps. The first involves the representation of the aerosol number and chemical composition distribution with respect to size, and calculation of the number concentration of droplets that can potentially form at a certain level of supersaturation (the cloud condensation nucleus, CCN, spectrum). Modified Köhler theory, which embodies effects of surfactant and slightly soluble species, is used to compute the supersaturation needed for a CCN to activate [*Shulman et al.*, 1996; *Laaksonen et al.*, 1998]. In the second step, the CCN spectrum is included within the framework of an adiabatic cloud parcel model, with specified updraft velocity (or cooling rate), to compute the maximum supersaturation, s_{max}, of the cloud parcel. The number concentration of nucleated drops is calculated from Equation 8.

Considerable attention has been given to the approximation used in estimating the droplet size, at the point of parcel maximum supersaturation (which is a key parameter, as it controls the condensation rate). A common assumption taken is that the CCN

grows instantaneously to its critical diameter, when the parcel supersaturation becomes equal to the CCN's critical supersaturation, i.e. the activation process is not kinetically limited. When this condition is not satisfied, it can be a source of significant error in prediction of the number of activated droplets [*Nenes et al.*, 2001]; this is one of the issues addressed in the new parameterization. We would like to note that the previously described kinetic limitation mechanism has long been known (e.g., *Jensen and Charlson* [1984]; *Chuang et al.* [1997]); this was called "inertial" kinetic limitation by *Nenes et al.* [2001]. (In addition to the "inertial" mechanism, *Nenes et al.* [2001] also identified two other kinetic limitation mechanisms, the "de-activation" and "evaporation" mechanisms. In this study, we only consider the "inertial" mechanism, as that can have a substantial effect on the condensation rate and thus s_{max}).

4.1. Computation of parcel maximum supersaturation

In an adiabatic parcel, the rate of change of the supersaturation, s, for a cloud parcel that ascends with a constant vertical velocity, V is [*Pruppacher and Klett*, 1997; *Seinfeld and Pandis*, 1998]:

$$\frac{ds}{dt} = \alpha V - \gamma \frac{dW}{dt} \tag{9}$$

where

$$\alpha = \frac{gM_w\Delta H_v}{c_p RT^2} - \frac{gM_a}{RT}, \quad \gamma = \frac{pM_a}{p^s M_w} + \frac{M_w \Delta H_v^2}{c_p RT^2} \tag{10}$$

and where ΔH_v is the latent heat of condensation of water, T is the parcel temperature,

M_w is the molecular weight of water, g is the acceleration of gravity, M_a is the molecular weight of air, c_p is the heat capacity of air, p^s is the water saturation vapor pressure, p is the ambient pressure, dW/dt is the rate of condensation of liquid water onto the drops, and R is the universal gas constant.

The first term on the right hand side of Equation 9 expresses the tendency of supersaturation to increase from the cooling of the parcel, while the second term expresses the tendency of supersaturation to decrease because of depletion of water vapor by the activated droplets.

The rate of water condensation on the droplet population can be expressed as,

$$\frac{dW}{dt} = \frac{\pi}{2}\rho_w \int_0^s D_p^2 \frac{dD_p}{dt} n^s(s')ds' \tag{11}$$

where ρ_w is the density of water. By substituting Equation 11 into 9, we obtain,

$$\frac{ds}{dt} = \alpha V - \gamma \frac{\pi}{2}\rho_w \int_0^s D_p^2 \frac{dD_p}{dt} n^s(s')ds' \tag{12}$$

The parcel supersaturation reaches a maximum when water vapor availability from parcel cooling becomes equal to the depletion rate from the activated drops; this is expressed by setting ds/dt in Equation 12 equal to zero:

$$\alpha V - \gamma \frac{\pi}{2}\rho_w \int_0^{s_{max}} D_p^2 \frac{dD_p}{dt} n^s(s')ds' = 0 \tag{13}$$

The rate of growth of a drop of diameter D_p is determined from [*Seinfeld and Pandis*, 1998],

$$\frac{dD_p}{dt} = \frac{G}{D_p}(s - s_{eq}) \tag{14}$$

$$G = \frac{4}{\frac{\rho_w RT}{p_v^* D_v M_w} + \frac{\Delta H_v \rho_w}{k_a T\left(\frac{\Delta H_v M_w}{RT} - 1\right)}} \tag{15}$$

and k_a is the thermal conductivity of air, D_v is the water vapor diffusivity, and s_{eq} is the equilibrium supersaturation of the droplet.

With the assumption that beyond the point of activation, the growth rates are not significantly influenced by droplet curvature and solute effects, $s_{eq} = 0$, Equation 14 becomes [*Twomey*, 1959],

$$\frac{dD_p}{dt} = \frac{G}{D_p} s \tag{16}$$

One can integrate Equation 16 from time τ, when the parcel supersaturation is equal to the CCN critical supersaturation, to the time of maximum supersaturation, t_{max}, to give the droplet diameter at the time of s_{max},

$${D_p}^2 = D_p^2(\tau) + 2\int_{\tau}^{t_{max}} G s dt \tag{17}$$

By substituting Equations 17 and 16 into Equation 13, we obtain,

$$\frac{2\alpha V}{\pi\gamma\rho_w} - G s_{max} \int_0^{s_{max}} \left(D_p^2(\tau) + 2G\int_{\tau}^{t_{max}} s dt\right)^{1/2} n^s(s') ds' = 0 \tag{18}$$

Before proceeding further, we need to evaluate the integral in Equation 18, referred to herein after as $I(0, s_{max})$,

$$I(0, s_{max}) = G s_{max} \int_0^{s_{max}} \left(D_p^2(\tau) + 2G \int_\tau^{t_{max}} s dt \right)^{1/2} n^s(s') ds' \tag{19}$$

where the parameters in the parenthesis indicate the limits of integration. If $I(0, s_{max})$ is evaluated and substituted in Equation 18, the parcel maximum supersaturation can then be calculated, and subsequent substitution into 8 would yield cloud droplet number concentration.

4.2. Calculation of integral I.

An analytical expression for I is not possible, but I has two asymptotic limits. The first limit, I_1, is obtained when

$$D_p^2(\tau) << 2G \int_\tau^{t_{max}} s dt \tag{20}$$

In this limit, the CCN experience significant growth beyond the point where they are exposed to $s > s_c$. Note that the above approximation is used to derive the parameterization of *Twomey* [1959]. The supersaturation integral in Equation 19 can be evaluated using the lower bound of *Twomey* [1959],

$$\int_\tau^{t_{max}} s dt \approx \frac{1}{2\alpha V} (s_{max}^2 - s(\tau)^2) \tag{21}$$

where $s(\tau)$ is the parcel supersaturation at time τ. Substituting Equations 20, 21 and 5 into 19, we eventually obtain,

$$I_1(0, s_{max}) = \frac{s_{max} G^{3/2}}{(aV)^{1/2}} \sum_{j=1}^{i} \frac{N_j}{s_c^j - s_c^{j-1}} \left[\frac{x}{2} \left(s_{max}^2 - x^2 \right)^{1/2} + \frac{s_{max}^2}{2} Arc \sin \frac{x}{s_{max}} \right]_{x=s_c^{j-1}}^{x=s_c^j} \quad (22)$$

where the bracket signifies the difference between evaluation at $x = s_c^j$ and $x = s_c^{j-1}$, and, i is the section that contains s_{max} (i.e., $s_c^{i-1} \leq s_{max} \leq s_c^i$).

The second limit, I_2, of I is obtained when

$$D_p^2(\tau) >> 2G \int_\tau^t s dt \quad (23)$$

which physically means that the CCN do not experience significant growth beyond the point where they are exposed to $s > s_c$. A common assumption (used in the parameterization of *Ghan et al.* [1993]) is that $D_p(\tau)$ is equal to the critical diameter, $D_c = 2A/3s_c$, when the parcel s becomes equal to the particle s_c ($A = 4M_w\sigma/RT\rho_w$, and σ is the droplet surface tension at its critical diameter). This can be assumed when the timescale of particle growth is small compared to the rate at which supersaturation changes in the parcel [*Chuang et al.*, 1997]; this implies that the CCN is in equilibrium with the parcel supersaturation until the point of activation, hence will instantaneously grow to D_c when exposed to its critical supersaturation. (We will elaborate on the implications of this assumption subsequently.) Substitution of Equation 23 into Equation 19 (with the assumption $D_p(\tau) = D_c$) and evaluation of the integral yields,

$$I_2(s_c^1, s_{max}) = \frac{2G s_{max}}{3} \left[\sum_{j=2}^{i-1} \left(\frac{N_j A_j}{s_c^j - s_c^{j-1}} \right) \ln \frac{s_c^j}{s_c^{j-1}} + \left(\frac{N_i A_i}{s_c^i - s_c^{i-1}} \right) \ln \frac{s_{max}}{s_c^{j-1}} \right] \quad (24)$$

where A_j is an average A over section j. Note that j starts from 2, otherwise $I_2 \to \infty$ as $s_c^0 \to 0$. This asymptotic limit will not be a problem for the parameterization, as I_2 will always be used with a nonzero lower bound. In equation 24, i is the section that contains s_{max} (i.e., $s_c^{i-1} \leq s_{max} \leq s_c^i$).

4.3. The concept of "population splitting".

While neither of Equations 22 or 24 alone is expected to describe the behavior of all the CCN during their activation, it is reasonable to divide the CCN into two groups: those that would follow Equation 22, and others that would follow 24. This classification of CCN, which we call *population splitting*, will be used to approximate I,

$$I = I_1(0, s_{part}) + I_2(s_{part}, s_{max}) \tag{25}$$

The ordering of the two integrals is deliberate; I_1 is used for low s_c CCN, while I_2 is used for the remaining CCN. This ordering will be justified subsequently (in section 4.4). The upper bound of I_1 and the lower bound of I_2 in Equation 25 is termed the *partitioning critical supersaturation*, s_{part} (Figure 2). Physically, this supersaturation defines two populations of droplets: one for which $D_p \approx D_c$, and one for which either $D_p \gg D_c$ or $D_p \ll D_c$ (but still large enough to be considered a droplet). Note that Equation 25 assumes that for a given population, there is only one s_{part}. If s_{part} is known, the integral I can be evaluated and substituted into Equation 18; s_{max}, and N_d can then be calculated. The following sections develop the procedure used for calculating s_{part}.

4.4. Implementation of population splitting.

Numerical simulations with a cloud parcel model [*Nenes et al.*, 2001] reveal that s_{part} depends on s_{max}, V, and the CCN spectrum characteristics. We will now attempt to derive theoretical expressions for s_{part}. An obvious candidate for s_{part} is the critical supersaturation of the CCN population for which $D_p^2(\tau) = 2G\int_\tau^{t_{max}} sdt$. From Equation 21 and substituting $D_p(\tau) = 2A/3s_{part}$, we obtain,

$$\frac{4A^2}{9s_{part}^2} = \frac{G}{\alpha V}(s_{max}^2 - s_{part}^2) \tag{26}$$

where $A = 4M_w\sigma_w/RT\rho_w$, and σ_w is the surface tension of water. After some algebra, Equation 26 leads to the quartic equation,

$$p(s_{part}) = s_{part}^4 - s_{max}^2 s_{part}^2 + \frac{4A^2\alpha V}{9G} = 0 \tag{27}$$

If the descriminant, $\Delta = s_{max}^4 - \frac{16A^2\alpha V}{9G}$, of $p(s_{part})$ is non-negative, then Equation 27 has two real roots with respect to s_{part}:

$$\begin{aligned}\left(\frac{s_{part,1}}{s_{max}}\right)^2 &= \frac{1}{2}\left[1 - \left(1 - \frac{16A^2\alpha V}{9s_{max}^4 G}\right)^{1/2}\right] \\ \left(\frac{s_{part,2}}{s_{max}}\right)^2 &= \frac{1}{2}\left[1 + \left(1 - \frac{16A^2\alpha V}{9s_{max}^4 G}\right)^{1/2}\right]\end{aligned} \tag{28}$$

Each of the two roots, $s_{part1,2}$, expresses the s_c of those CCN for which their subsequent growth beyond activation is equal to D_c. These two characteristic s_c divide the CCN population into three groups: those with $s_c < s_{part,1}$, those with

$s_{part,2} < s_c < s_{part,1}$, and those with $s_{part,2} < s_c$. If a CCN has an s_c between $s_{part,1}$ and $s_{part,2}$, then $p(s_c) < 0$, which means that the CCN experiences significant growth after it attains its critical diameter. For other values of s_c, $p(s_c) > 0$, which means that the growth experienced by the CCN is smaller than its critical diameter. Note the latter does *not* mean that when $p(s_c) > 0$, the CCN size can be approximated by its critical size; further knowledge of droplet growth kinetics is needed for deciding whether this approximation can be used.

Of all the CCN that form droplets, those with the highest s_c have sizes close to their D_c. This is because i) high s_c CCN are less influenced by kinetic limitations and thus would be in equilibrium with parcel supersaturation until the point of activation, and ii) because they have the least time to grow beyond activation [*Nenes et al.*, 2001]. This condition is valid for particles which $s_c > s_{part,2}$. However, as s_c decreases, the time available for growth increases, and at some point, the droplet growth becomes large enough to substantially exceed the CCN critical diameter. This happens for the particles for which $s_{part,1} < s_c < s_{part,2}$. Apart from having the benefit of increased exposure time, a decrease in s_c also leads to a larger D_c; at the value of $s_c = s_{part,1}$, the subsequent growth beyond activation becomes equal to D_c; for lower s_c, D_c is larger than the growth experienced by the particle. Therefore, CCN for which $s_c < s_{part,1}$ are kinetically limited and do not attain their critical diameter; Equation 20 cannot be used to estimate the CCN size, as it never approaches its critical diameter (this is confirmed from simulations with a detailed adiabatic cloud model [*Nenes et al.*, 2001]). Therefore, approximating I with I_2 for the kinetically-limited CCN can lead to large biases because

their droplet size would be systematically overestimated by assuming $D(\tau) = D_c$.

Since those CCN, the growth of which is kinetically limited, have a small s_c, it is reasonable to approximate their driving force for droplet growth (Equation 14), $s - s_{eq}$, with s, even before they activate (this is because, $s_{eq} \leq s_c \approx 0$). The growth of such a particle can then be expressed as,

$$D_p^2 \approx 2G \int_{\tau}^{t_{max}} s dt \tag{29}$$

which is equivalent to Equation 20. Thus, I_1 is used to approximate I for CCN with $s_c < s_{part,1}$. On this basis, $s_{part} = s_{part,2}$ and the following can be said,

$$\begin{aligned} \left(\frac{s_c}{s_{max}}\right) \leq \left(\frac{s_{part}}{s_{max}}\right) \Rightarrow D_p^2(\tau) << 2G \int_{\tau}^{t_{max}} s dt \Rightarrow I \approx I_1 \\ \left(\frac{s_c}{s_{max}}\right) > \left(\frac{s_{part}}{s_{max}}\right) \Rightarrow D_p^2(\tau) >> 2G \int_{\tau}^{t_{max}} s dt \Rightarrow I \approx I_2 \end{aligned} \tag{30}$$

The descriminant Δ expresses the extent of kinetic limitations throughout the droplet formation, and depends on s_{max} (which depends primarily on V and CCN characteristics), V, and the timescale of water vapor diffusion (embodied in G). $\Delta = 0$ marks a boundary between two growth regimes: one where most CCN are free from kinetic limitations ($\Delta > 0$) and one in which kinetic limitations are dominant ($\Delta < 0$). As Δ increases, $s_{part,1} \rightarrow 0$ and $s_{part,2} \rightarrow s_{max}$, so that more of the CCN attain sizes larger than their critical diameter; this means that fewer CCN are subject to kinetic limitation. (This is consistent with the analysis of *Nenes et al.* [2001], as increasing parcel s_{max} and V leads to rapid particle growth and therefore to a decrease

in kinetic limitations.) The rules in Equation 30 indicate that for a non-negative Δ, $\left(\frac{s_{part}}{s_{max}}\right) \geq \sqrt{0.5}$. In this regime, s_{part} decreases with decreasing s_{max}.

When $\Delta < 0$, Equation 27 is without real roots; under these conditions, kinetic limitations in droplet growth are strong throughout the entire CCN population. Of all the CCN, those with the highest s_c would tend to have size of order D_c, since: i) the timescale of activation decreases with particle size (or with increasing s_c) [*Chuang et al.*, 1997], and, ii) $p(s_c)$ is closest to zero as $s_c \rightarrow s_{max}$. Therefore, for CCN of high s_c, I_2 can be used to approximate I. The lower s_c particles can be considerably smaller than their critical size, but with small s_c, their growth, as before, can be represented by Equation 29; I_1 will therefore be used to approximate I. Consequently, Equations 30 will still be used to approximate I, even if $\Delta < 0$. Based on the previous discussion we anticipate that fewer CCN can attain their critical diameter as the parcel maximum supersaturation decreases; numerical simulations support this expectation. s_{part} increases with decreasing s_{max} and is calculated from the following correlation, derived from regression of a large set of empirical s_{part} that reproduce the predictions of a detailed microphysics model,

$$\frac{s_{part}}{s_{max}} = min\left\{0.666 \times 10^7 A s_{max}^{-0.3824}, 1.0\right\} \tag{31}$$

The simulations on which Equation 31 is based were chosen so that $\Delta < 0$. In generating numerical values for Equation 31, the mass accommodation coefficient of water vapor on aqueous drops is equal to 1.0, and $T = 283$ K. Equation 31 indicates

that as $s_{max} \rightarrow 0$, $s_{part}/s_{max} \rightarrow 1$, meaning that as the s_{max} decreases, fewer and fewer of the CCN can attain their critical diameter. All the rest are kinetically-limited.

Combination of the two expressions for calculating s_{part} (Equation 31 for $\Delta < 0$ and $s_{part} = s_{part,2}$ for $\Delta > 0$) displays physically expected behavior. Figure 3 shows s_{part}/s_{max} as a function of s_{max}. Each line corresponds to a different value of updraft velocity, V. Given that each curve in Figure 3 is for constant updraft velocity V, s_{max} varies only because of changes in aerosol concentration; Figure 3 thus displays the Twomey effect on s_{part}. Note that there are regions for which s_{part} is insensitive to changes in s_{max}; we would expect that simple parameterizations perform well in these regions, as they do not exhibit implicit dependence on s_{max}. At large values of s_{max}, $s_{part}/s_{max} \rightarrow 1$, indicating that the vast majority of the CCN are not subject to kinetic limitations. For lower values of s_{max}, s_{part}/s_{max} reaches a minimum; a further decrease in s_{max}, however, reverses the trend for s_{part}/s_{max}, as explained above. An activation parameterization is severely tested in regions where s_{part} changes rapidly.

It is also important to examine the behavior of s_{part}, for constant aerosol concentration and variable updraft velocity. To do so, we need information regarding the relationship between aerosol concentration, V and s_{max}. This is accomplished by using a numerical parcel activation model for the four aerosol types shown in Table 2. The results are shown in Figure 4. Clearly we can see that for marine-type aerosols, s_{part} is close to unity (meaning that the vast majority of the droplets attain sizes larger than their critical diameter) for all updraft velocities; the other extreme is the urban aerosol, which always experiences significant kinetic limitations. For the distribution used here,

between 20% to 40% of the particles do not reach critical size at any updraft velocity. These percentages agree well with the numerical results of *Nenes et al.* [2001] for the same aerosol size distributions; this is verification that the procedure used for calculating s_{part} is realistic. (Note that the correlation was derived from many simulations).

4.5. Final form of aerosol activation parameterization

After evaluation of Equation 25, and substitution into Equation 18, we obtain the final form of the parameterization, which is a nonlinear algebraic equation for the maximum supersaturation of the cloud parcel,

$$\frac{\pi}{2}\frac{\gamma\rho_w G s_{max}}{aV}\left\{\int_0^{s_{part}} D_p n^s(s')ds' + \int_{s_{part}}^{s_{max}} D_p n^s(s')ds'\right\} - 1 = 0 \tag{32}$$

where,

$$\int_0^{s_{part}} D_p n^s(s')ds' = \left(\frac{G}{aV}\right)^{1/2} \sum_{j=1}^{i_{part}} \frac{N_j}{s_c^j - s_c^{j-1}}\left[\frac{x}{2}\left(s_{max}^2 - x^2\right)^{1/2} + \frac{s_{max}^2}{2} Arc\sin\frac{x}{s_{max}}\right]_{x=s_c^{j-1}}^{x=s_c^j}$$

$$\int_{s_{part}}^{s_{max}} D_p n^s(s')ds' = \frac{2}{3}\left[\sum_{j=i_{part}}^{i_{max}-1}\left(\frac{N_j A_j}{s_c^j - s_c^{j-1}}\right)\ln\frac{s_c^j}{s_c^{j-1}} + \left(\frac{N_{i_{max}} A_{i_{max}}}{s_c^{i_{max}} - s_c^{i_{max}-1}}\right)\ln\frac{s_{max}}{s_c^{i_{max}-1}}\right]$$

where i_{part} is the section boundary closest to s_{part} (implementation of population splitting within an aerosol section is straightforward), and, i_{max} is the boundary closest to s_{max} with $s_{max} \le s_{i_{max}}$ (Figure 2). The calculation of s_{part} is carried out using either Equation 28 (when $\Delta \ge 0$) or Equation 31 (when $\Delta < 0$).

The procedure for using the parameterization is illustrated in Figure 5. Equation 32 is solved for s_{max} using the bisection method. All physical properties are evaluated

at cloud base conditions. The number of droplets is computed from Equation 8.

We would like to point out that the complexity of the integrals in equation 32 arises from using a sectional representation for the CCN spectrum (equation 6), and not from the procedure used to develop the parameterization (i.e., the concept of populations splitting, and calculation of s_{split}). The formulation for other size distributions (e.g., lognormal) can be much simpler than equation 6, but is beyond the scope of this paper.

5. Evaluation of new parameterization

5.1. Activation conditions considered.

The performance of the new parameterization will be evaluated by comparing the predicted cloud droplet number concentrations with those of a full numerical activation adiabatic cloud parcel model [*Nenes et al.*, 2001]. The parameterization is tested for a large number of aerosol size distributions and updraft velocities (about 200 cases total), which encompass the wide variety of tropospheric aerosols. For convenience, size distributions are taken to be of the single or multiple log-normal form,

$$\frac{dn\left(D_p\right)}{d\ln D_p} = \sum_{i=1}^{n_m} \frac{N_i}{\sqrt{2\pi}\ln\sigma_i} \exp\left[-\frac{\ln^2\left(D_p/D_{g,i}\right)}{2\ln^2\sigma_i}\right] \tag{33}$$

where N_i is the aerosol number concentration, $D_{g,i}$ the number mode diameter, σ_i is the geometric standard deviation for mode i, and n_m is the number of modes in the distribution.

For single mode aerosol, we consider a wide range in number concentration, mode

diameter, and dispersions. The range in mode diameter and number concentration is appropriate for accumulation mode particles, which comprise most CCN. Table 1 summarizes the characteristics of the mode radii, number concentrations, and updrafts examined.

For multiple mode aerosol, we have selected four of the *Whitby* [1978] trimodal representations, namely the marine, clean continental, average background, and urban aerosol (Table 2). The size distributions refer to dry size, while the chemical composition of the aerosol is assumed to be pure ammonium sulfate. To evaluate the ability of the new parameterization to capture the effect of surface-active organics, we also perform simulations for an aerosol that has the *Whitby* [1978] marine aerosol size distribution, which is assumed to be composed of 80% by mass $(NH_4)_2SO_4$ and 20% organic that displays surface active behavior. The aerosol organic component is a reconstruction of chemical composition observed in Po Valley fogs and is assumed to be composed of 18% (by mass) levoglucosan ($C_6H_{10}O_5$, density = 1600 kg m^{-3}, van't Hoff factor = 1), 41% (by mass) succinic acid ($C_6O_4H_6$, density = 1572 kg m^{-3}, van't Hoff factor = 3), and 41% (by mass) fulvic acid [*US Geological Survey*, 1979], ($C_{33}H_{32}O_{19}$, density = 1500 kg m^{-3}, van't Hoff factor = 5 *Nenes et al.* [2002a]). The surface tension behavior of this organic is assumed to follow the correlation of *Facchini et al.* [1999]. Finally, to test the performance of the parameterizations under conditions of strong kinetic limitations, we examine the same size distributions with the concentrations doubled. The characteristics of the simulations are summarized in Table 3.

In the numerical parcel simulations, particles are assumed initially to be in

equilibrium at a relative humidity of 98%, and P,T as specified in Tables 1 and 3. For both the new parameterization and numerical parcel model, we consider 200 size bins spaced equally in log diameter. Using a size range between $D_{p,g}/10\sigma$ and $10\sigma D_{p,g}$ covers total particle number to within 10^{-7}%. The simulations exhibit little sensitivity with respect to initial relative humidity and use of a denser grid. Using 200 bins for both the parameterization and the parcel model ensures that differences in droplet number between the two is not due to discretization error.

When using the parameterization, the droplet number is calculated from Equation 8. When using the parcel model, the droplet concentration is calculated using the criterion of *Nenes et al.* [2001], which is to find the CCN of highest s_c that strictly activates (i.e. exceeds its critical diameter); anything larger than this CCN is counted as a drop. Note that this definition accounts for kinetic limitations; large CCN that have not attained their critical diameter are considered as droplets, but not those that deactivate and become interstitial aerosol. Droplet concentration is evaluated at 250 m above cloud base.

5.2. Comparison of new parameterization with parcel model.

Figure 6 displays the fraction of aerosol that becomes droplets (termed as "activation ratio"), as predicted by the new parameterization and the parcel model. For the wide variety of aerosol and updraft velocities considered, the activation ratio ranges between 10^{-3} to 1.0. Most of the predicted values are very close to the 1:1 line, and do not display significant systematic biases over the range of activation ratios;

this shows that the parameterization performs well regardless of the steepness of the CCN spectrum (at low activation ratios, the spectrum is steep, while at high activation ratios, the spectrum is not). This also indicates that the parameterization is capable of treating highly complex and "irregular" CCN spectra, which deviate substantially from the smoothness of CCN spectra that correspond to log-normal size distributions. We do note however, that although there is scatter about the 1:1 line, more frequently the activated fraction tends to be underestimated. This is because the maximum supersaturation for these cases is slightly underpredicted, and leads to a corresponding underprediction in droplet number. s_{max} is underpredicted, because the condensation rate is slightly overpredicted.

Figure 7 displays the droplet number concentration as predicted by the new parameterization and the parcel model. The range of droplet concentrations covers the entire range observed in clouds (e.g. *Boucher and Lohmann* [1995]; *Gultepe and Isaac* [1996]). The predicted droplet number follows the 1:1 line closely. There are no regions with a variable systematic bias in the predictions, indicating that the parameterization performs well, regardless of the extent of kinetic limitations throughout the droplet population. Confirmation of this can be attained by evaluating the performance of the parameterization for the two Δ regimes. This is shown in Figure 8, which is the same as Figure 7, but with the points colored according to the value of Δ. Most of the points examined are for $\Delta \geq 0$, but clearly the two regimes exhibit equivalent scatter around the 1:1 line; this is a strong indication that the parameterization is insensitive to the extent of kinetic limitations.

It is important to evaluate the performance of the parameterization in predicting the parcel s_{max} (Figure 9). The range of maximum parcel supersaturations covers that predicted for most clouds; for most cases, the parcel supersaturation is well captured. It is notable that the parameterization captures even the urban and background aerosols, which are subject to strong kinetic limitations (which account for roughly half of the multimodal cases examined). Particularly challenging are the TM2-U simulations. The s_{max} in these cases is very small (on the order of 0.01%), and errors in this quantity can lead to large biases in predicted N_d; the parameterization nonetheless reproduces the parcel simulations very well. It should be noted however that the parameterization (for these conditions) tends to slightly underestimate s_{max}.

Figures 6 to 9 display some scatter around the 1:1 line. It is important to examine how significant this scatter is, on average and on a per-case basis, as we can gain further insight into possible systematic biases. Table 4 displays the statistics of the ratio of parameterized N_d to the N_d calculated from the parcel model; if the parameterization perfectly captured the parcel simulations, this ratio would be 1.0. The overall average ratio is about 0.95, with a standard deviation of 0.1. Grouping the results according to aerosol case and Δ regime, we note that the performance is excellent for all the multimodal aerosols (TM1, TM2), despite the fact that about half of the cases involve significant kinetic limitations. Some of the single mode cases perform less optimally, but still are quite close to the cloud parcel predictions. The statistics for the two Δ regimes are about the same; the fact that $\Delta < 0$ has double the standard deviation of $\Delta \geq 0$ is likely a result of the smaller statistical sample. In any case, the standard deviation for

all of the statistics is small, which indicates the robustness of the parameterization.

Finally, we address the performance of the new parameterization for an aerosol containing an organic species. Capturing the activation behavior of these CCN is more difficult than those containing only soluble salt and insoluble substances, as the presence of an organic species within CCN can affect the activation behavior in many ways: the organic can contribute soluble material (e.g. *Shulman et al.* [1996]), can alter the droplet surface tension (e.g., *Shulman et al.* [1996]; *Facchini et al.* [1999], and potentially affect the droplet growth kinetics (e.g., *Feingold and Chuang* [2002]; *Nenes et al.* [2002a]). Here we will focus on the solute and surface tension effects. Given that organics which can substantially affect surface tension can also be highly soluble (e.g., humic-like substances), we will assume that the organic is completely soluble (the overall effect on activation, at least for the conditions examined here, do not change appreciably even if the solubility changes considerably [*Nenes et al.*, 2002a]). Under these conditions, the challenge for the organic-containing CCN is to calculate the surface tension at the point of activation (which varies with aerosol size and composition). This difficulty is overcome by the sectional representation of the aerosol, as the effect of the surface-active species can be included in the calculation of the s_c of each CCN section. We simulate the activation of an aerosol assumed to follow the *Whitby* [1978] marine aerosol size distribution (Table 2), composed of 80% by mass $(NH_4)_2SO_4$ and 20% by mass organic surfactant (with a composition as given before). Figure 10 displays the activation ratio as a function of updraft velocity, as predicted by the parameterization and the parcel model. The parameterization captures well the activation behavior of

the aerosol. Excluding the effects on surface tension results in the expected decrease in droplet number.

5.3. Comparison with other parameterizations.

The new parameterization is tested against the performance of the *Abdul-Razzak and Ghan* [2000] parameterization in reproducing the results of the parcel model. These parameterizations were chosen for comparison as they are the most comprehensive formulations available in the literature. We would like to point out that the new and the *Abdul-Razzak et al.* [1998] and *Abdul-Razzak and Ghan* [2000] parameterizations are fundamentally different in their representation of the CCN spectrum. The former uses a sectional representation, and the latter two, a modal representation (i.e., an exact analytical integration over a lognormal size distribution). We ensured that the differences in droplet number between the parameterizations are only from their treatment of the activation process by using 200 size bins for the new parameterization (and parcel model). This way, when approximating the lognormal distribution with a series of size sections, the discretization error is very small (less than 1% in droplet number).

Figure 11 displays the fraction of aerosol that becomes droplets, as predicted by the *Abdul-Razzak and Ghan* [2000] parameterization and the parcel model. For most cases, these parameterizations perform well, but numerous cases deviate considerably from the 1:1 line. This behavior is also seen in the parameterized s_{max} (not shown). For a given size distribution, the deviations seem to become larger as the activation ratio decreases,

that is the steep-slope region of the CCN activation spectrum. Figure 12 displays the droplet number for the same conditions as in Figure 11. The deviations from the 1:1 line do not seem to follow any systematic behavior, so they are less likely to be controlled by kinetic limitations (this is understandable, as the parameterization is fitted to numerical parcel simulations, thus implicitly accounting for kinetic limitations). Actually, the opposite is occurring: the predictions for the marine aerosols deviate notably from the parcel simulations. *Abdul-Razzak and Ghan* [2000] report that errors are expected from the parameterization when the modal diameters differ by about an order of magnitude. The nuclei and accumulation modes in the marine and continental aerosol runs vary by a factor of 7, and for the urban and background aerosol, by a factor of 5; therefore, errors are expected. The deviations do not seem to be focused in any particular region of droplet number concentration, but rather for certain combinations of mode dispersion and updraft velocity. This behavior indicates that the biases most likely originate from the correlation used in the parameterization.

6. Conclusions

A new aerosol activation parameterization has been developed, based on a generalized sectional representation of aerosol size and composition. The maximum supersaturation needs to be determined first by numerically solving an algebraic equation, and then the droplet number concentration is computed from the supersaturation spectrum. The flexibility of the parameterization and comprehensive treatment of the droplet activation justify the additional computational effort.

We introduce the concept of "population splitting", in which the CCN that form droplets are divided into two separate populations: those which have a size close to their critical diameter, and those that do not. We also explicitly introduce kinetic limitations on droplet growth. For a wide range of CCN activation conditions, the parameterization is free from any empirical information or correlations derived from detailed numerical simulations. There are certain conditions for which an empirically derived correlation is utilized; this is required whenever most of the activated CCN are kinetically limited. Whether the empirical information is needed or not is determined by a parameter that indicates the extent of kinetic limitations (defined as the "descriminant criterion", Δ).

Predictions of the parameterization are extensively compared against those of a detailed cloud parcel activation model, for a variety of aerosol activation conditions that cover a wide range of chemical variability and CCN concentrations. The parameterization closely tracks the parcel model simulations, while the computational burden of the parameterization is more than three orders of magnitude less than that of the parcel model itself. The new parameterization displays superior performance, in both accuracy and robustness, when compared to existing parameterizations. Decreased reliance on empirical information does not diminish the performance of the parameterization; on the contrary, it seems to enhance its robustness.

The new parameterization, in the formulation presented in this paper, can treat all types of aerosol that follow Köhler theory; as no restriction of an explicit link between dry size and critical supersaturation is needed, the parameterization can treat internally or externally mixed aerosol, with size varying composition, including the effects of

surface active species (organics), insoluble species and slightly soluble species. The current formulation can even treat recently identified effects, such as the heating of CCN from the presence of black carbon [*Conant et al.*, 2002; *Nenes et al.*, 2002b]. The possibilities do not stop here. The structure of the parameterization allows for further extension, such as explicit treatment of condensable gases and organic species that exhibit slow growth kinetics, and including entrainment in the parcel (non-adiabatic activation). Although much is still unknown about the effect of organic species on droplet activation, the ability to parameterize their possible effects is highly desirable, as it establishes the framework for a comprehensive assessment of the aerosol indirect effect in global climate models.

Acknowledgments. This work was supported by the NASA Earth Observing System-Interdiciplinary Science program (NASA EOS-IDS) and the Office of Naval Research grant N00014-96-1-0119. We would also like to thank T. Rissman for assistance with some of the ARG parameterization calculations.

References

Abdul-Razzak, H., and S. Ghan, A parameterization of aerosol activation 2. Multiple aerosol types, *J. Geophys. Res.*, *105*, 6837–6844, 2000.

Abdul-Razzak, H., and S. Ghan, A parameterization of aerosol activation 3. Sectional representation, *J. Geophys. Res.*, *107*, 2002.

Abdul-Razzak, H., S. Ghan, and C. Rivera-Carpio, A parameterization of aerosol activation. part I: Single aerosol type, *J. Geophys. Res.*, *103*, 6123–6132, 1998.

Adams, P. J., and J. H. Seinfeld, Predicting global aerosol size distributions in general circulation models, *J. Geophys. Res.*, *in press*, 2002.

Boucher, O., and U. Lohmann, The sulfate-CCN-cloud albedo effect - A sensitivity study with 2 general-circulation models, *Tellus B*, *47*, 281–300, 1995.

Charlson, R., J. Seinfeld, A. Nenes, M. Kulmala, A. Laaksonen, and M. Facchini, Atmospheric science - reshaping the theory of cloud formation, *Science*, *292*, 2025–2026, 2001.

Chuang, C. C., and J. E. Penner, Effects of anthropogenic sulfate on cloud drop nucleation and optical properties, *Tellus B*, *47*, 566–577, 1995.

Chuang, P., R. Charlson, and J. Seinfeld, Kinetic limitation on droplet formation in clouds, *Nature*, *390*, 594–5962, 1997.

Cohard, J., J. Pinty, and C. Bedos, Extending Twomey's analytical estimate of nucleated cloud droplet concentrations from CCN spectra, *J. Atmos. Sci.*, *55*, 3348–3357, 1998.

Cohard, J., J. Pinty, and K. Suhre, On the parameterization of activation spectra

from cloud condensation nuclei microphysical properties, *J. Geophys. Res.*, *105*, 11,753–11,766, 2000.

Conant, W., A. Nenes, and J. Seinfeld, Black carbon radiative effect on cloud microphysics and implications for the aerosol indirect effect: 1. Extended Köhler theory, *J. Geophys. Res.*, *107*, doi: 10.1029/2002JD002,094, 2002.

Facchini, M., M. Mircea, S. Fuzzi, and R. Charlson, Cloud albedo enhancement by surface-active organic solutes in growing droplets, *Nature*, *401*, 257–259, 1999.

Feingold, G., and P. Chuang, Analysis of the influence of film-forming compounds on droplet growth: Implications for cloud microphysical processes and climate, *J. Atmos. Sci.*, *59*, 2006–2018, 2002.

Feingold, G., and A. Heymsfield, Parameterizations of condensational growth of droplets for use in general circulation models, *J. Atmos. Sci.*, *49*, 2325–2342, 1992.

Flossmann, A., W. Hall, and H. Pruppacher, A theoretical study of the wet removal of atmospheric pollutants: Part I: The redistribution of aerosol particles capture through nucleation and impaction scavenging by growing cloud drops, *J. Atmos. Sci.*, *42*, 583–606, 1985.

Ghan, S., C. Chuang, and J. Penner, A parameterization of cloud droplet nucleation. part I: Single aerosol species, *Atmos. Res.*, *30*, 197–222, 1993.

Ghan, S., C. Chuang, R. Easter, and J. Penner, A parameterization of cloud droplet nucleation .2. Multiple aerosol types, *Atmos. Res.*, *36*, 39–54, 1995.

Ghan, S., L. Leung, R. Easter, and H. Abdul-Razzak, Prediction of cloud droplet number in a general circulation model, *J. Geophys. Res.*, *102*, 21,777–21,794, 1997.

Gultepe, I., and G. Isaac, The relationship between cloud droplet and aerosol number concentrations for climate models, *Int. J. Climatol.*, *16*, 941–946, 1996.

Intergovernmental Panel on Climate Change (IPCC), *Climate Change (2001): The Scientific Basis*, Cambridge University Press, UK, 2001.

Jensen, J., and R. Charlson, On the efficiency of nucleation scavenging, *Tellus B*, *36*, 367–375, 1984.

Khvorostyanov, V., and J. Curry, A simple analytical model of aerosol properties with account for hygroscopic growth 1.Equilibrium size spectra and cloud condensation nuclei activity spectra., *J. Geophys. Res.*, *104*, 2175–2184, 1999.

Kiehl, J., Climate change - Solving the aerosol puzzle, *Science*, *283*, 1273, 1999.

Kiehl, J. T., T. L. Schneider, P. J. Rasch, M. C. Barth, and J. Wong, Radiative forcing due to sulfate aerosols from simulations with the National Center for Atmospheric Research Community Climate Model, Version 3, *J. Geophys. Res.*, *105*, 1441–1457, 2000.

Laaksonen, A., P. Korhonen, M. Kulmala, and R. Charlson, Modification of the Köhler equation to include soluble trace gases and slightly soluble substances, *J. Aerosol Sci.*, *155*, 853–862, 1998.

Lohmann, U., J. Feichter, C. Chuang, and J. Penner, Prediction of the number of cloud droplets in the ECHAM GCM, *J. Geophys. Res.*, *104*, 9169–9198, 1999.

Nenes, A., S. Ghan, H. Abdul-Razzak, P. Chuang, and J. Seinfeld, Kinetic limitations on cloud droplet formation and impact on cloud albedo, *Tellus B*, *53*, 133–149, 2001.

Nenes, A., R. Charlson, M. Facchini, M. Kulmala, A. Laaksonen, and J. Seinfeld, Can

chemical effects on cloud droplet number rival the first indirect effect?, *Geophys. Res. Lett.*, *24*, doi: 10.1029/2002GL015,295, 2002a.

Nenes, A., W. Conant, and J. Seinfeld, Black carbon radiative effect on cloud microphysics and implications for the aerosol indirect effect: 2. Cloud microphysics, *J. Geophys. Res.*, *107*, doi: 10.1029/2002JD002,101, 2002b.

Pruppacher, H., and J. Klett, *Microphysics of Clouds and Precipitation*, 2nd ed., Kluwer Academic Publishers, Boston, 1997.

Seinfeld, J., and S. Pandis, *Atmospheric chemistry and physics: from air pollution to climate change*, John Wiley, New York, 1998.

Shulman, M., M. Jacobson, R. Charlson, R. Synovec, and T. Young, Dissolution behaviour and surface tension effects of organic compounds in nucleating cloud droplets, *Geophys. Res. Lett.*, *23*, 277–280, 1996.

Squires, P., and S. Twomey, The relation between cloud droplet spectra and the spectrum of cloud nuclei, in *Physics of Precipitation, in Geoph. Monogr. Ser.*, 1960.

Twomey, S., The nuclei of natural cloud formation. II. The supersaturation in natural clouds and the variation of cloud droplet concentration., *Geofisica pura e applicata*, *43*, 243–249, 1959.

US Geological Survey, Suwanee River certified FA standards., *Report 87-557*, 1979.

Whitby, K., The physical characteristics of sulfur aerosols, *Atmos. Environ.*, *12*, 135–159, 1978.

Zhang, Y., R. Easter, S. Ghan, and H. Abdul-Razzak, Impact of aerosol size representation on modeling aerosol-cloud interactions, *J. Geophys. Res.*, *in press*, 2002.

A. Nenes, Schools of Earth and Atmospheric Sciences and Chemical Engineering, Georgia Institute of Technology, Atlanta GA, 30332. (e-mail: nenes@eas.gatech.edu)

J. H. Seinfeld, Department of Chemical Engineering, California Institute of Technology, Pasadena CA, 91125. (e-mail: seinfeld@caltech.edu)

Received _____

Figure Captions

Figure 1. Illustration of the sectional representation of (a) aerosol number distribution, $n^d(D_p)$, and (b) supersaturation distribution, $n^s(D_p)$.

Figure 2. Illustration of the two sub-populations used in developing the parameterization.

Figure 3. s_{part}/s_{max} as a function of s_{max}. Each curve corresponds to a constant updraft velocity.

Figure 4. s_{part}/s_{max} as a function of updraft velocity. Each curve corresponds to one of the aerosol types in Table 2. s_{max} is computed using the numerical parcel model of *Nenes et al.* [2001].

Figure 5. Parameterization algorithm.

Figure 6. Fraction of aerosol that become droplets, as predicted by the new parameterization and the cloud parcel model.

Figure 7. Droplet number concentration, as predicted by the new parameterization and the cloud parcel model.

Figure 8. Droplet number concentration, as predicted by the new parameterization and the cloud parcel model. The points are colored according to the value of Δ.

Figure 9. Maximum parcel supersaturation, as predicted by the new parameterization and the cloud parcel model.

Figure 10. Activated droplet ratio, as a function of updraft velocity. Both the cloud parcel model and parameterization results (with and without the effect of the organic from changes in surface tension) are shown. The parcel model simulations include surface tension effects from the dissolved organic. Marine aerosol composed of 80% $(NH_4)_2SO_4$ and 20% organic surfactant is used. The organic surfactant behavior is described in the text.

Figure 11. Fraction of aerosol that become droplets, as predicted by the *Abdul-Razzak and Ghan* [2000] parameterization and the cloud parcel model.

Figure 12. Droplet number concentration, as predicted by the *Abdul-Razzak and Ghan* [2000] parameterization and the cloud parcel model.

Tables

Table 1. Characteristics of single log-normal aerosol distribution runs. Pressure is 800 mbar, and temperature is 283 K.

Simulation set	$D_{g,i}$ (μm)	N_i (cm^{-3})	σ_i	V (m s^{-1})	# of points[a]
SM1[b]	0.02	200	2.5	0.1 - 10.0	18
SM2	0.02	1000	2.5	0.1 - 10.0	18
SM3	0.02	1000	1.5	0.1 - 10.0	18
SM4	0.2	200	2.5	0.1 - 10.0	18
SM5	0.02	10000	2.5	0.1 - 10.0	18
SM6	0.04-0.20	100 - 1000	2.0	0.1 - 3.0	72

[a] i.e. number of simulations considered for the specified range of parameters.

[b] "SM" denotes Single Mode.

Table 2. Aerosol distribution parameters ($D_{g,i}$ in μm, N_i in cm^{-3}) [*Whitby*, 1978]

Aerosol type	Nuclei Mode			Accumulation Mode			Coarse Mode		
	$D_{g,1}$	σ_1	N_1	$D_{g,2}$	σ_2	N_2	$D_{g,3}$	σ_3	N_3
Marine	0.010	1.6	340	0.070	2.0	60	0.62	2.7	3.1
Clean Continental	0.016	1.6	1000	0.068	2.1	800	0.92	2.2	0.72
Average Background	0.016	1.7	6400	0.076	2.0	2300	1.02	2.16	3.2
Urban	0.014	1.8	106000	0.054	2.16	32000	0.86	2.21	5.4

Table 3. Characteristics of multiple log-normal aerosol distribution simulations. The range in updraft velocity examined is 0.1 - 3.0 m s^{-1}. Pressure is 900 mbar, and temperature is 273 K.

Simulation set	Aerosol type	# of points[a]	Description.
TM1[b]-M[c]	Marine	4	Distribution from Table 2
TM1-C	Clean Continental	4	Distribution from Table 2
TM1-B	Average Background	4	Distribution from Table 2
TM1-U	Urban	4	Distribution from Table 2
TM2-M	Marine	4	TM1-M concentration doubled
TM2-C	Clean Continental	4	TM1-C concentration doubled
TM2-B	Average Background	4	TM1-B concentration doubled
TM2-U	Urban	4	TM1-U concentration doubled
TM3	Marine	4	TM1-M concentrations; surfactant present

[a] i.e. number of simulations considered for the specified range of parameters.

[b] "TM" stands for Tri-Modal.

[c] "M" for Marine, "C" for Continental, "B" for Background, and "U" for Urban aerosol.

Table 4. Statistics of the ratio of N_d calculated from new parameterization to N_d calculated from parcel model.

Simulation Set	Average Ratio	Minimum Ratio	Maximum Ratio	Standard Deviation	# of points (% with $\Delta < 0$)
TM1(all)	0.9332	0.7242	1.0838	0.1137	16 (44)
TM2(all)	0.9159	0.6864	1.0907	0.1284	16 (56)
SM1	0.8819	0.7983	0.9634	0.0530	18 (0)
SM2	0.7923	0.6356	0.9112	0.0722	18 (0)
SM3	0.7333	0.6298	0.8115	0.0494	18 (0)
SM4	1.0204	0.9720	1.2954	0.0782	18 (5)
SM5	0.6955	0.6222	0.7673	0.0406	18 (5)
SM6	0.9780	0.7481	1.1587	0.0854	72 (26)
$\Delta < 0$	0.9082	0.6864	1.2954	0.1461	37 (100)
$\Delta \geq 0$	0.9838	0.7975	1.1530	0.0704	161 (0)
Total	0.9582	0.6864	1.2954	0.1080	198 (19)

Figures

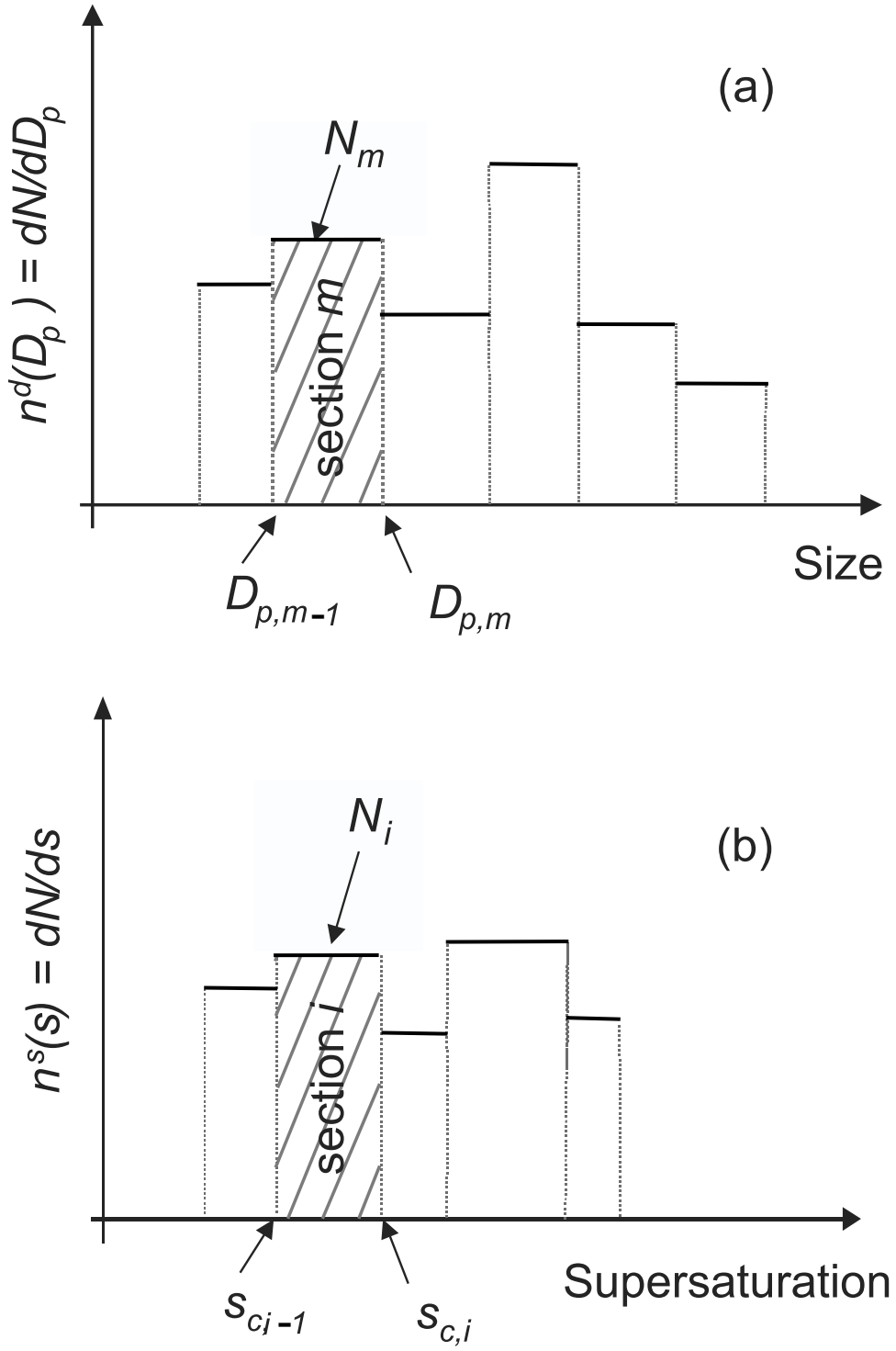

Figure 1. Illustration of the sectional representation of (a) aerosol number distribution, $n^d(D_p)$, and (b) supersaturation distribution, $n^s(D_p)$.

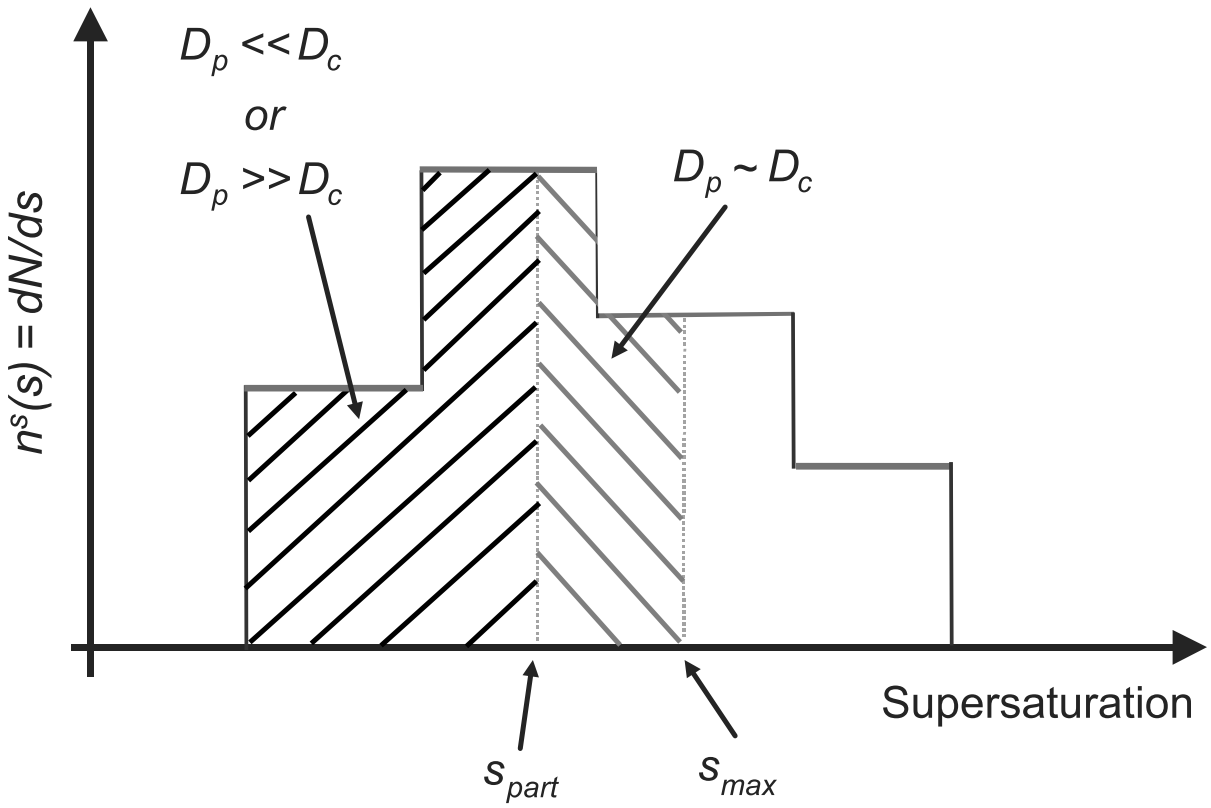

Figure 2. Illustration of the two sub-populations used in developing the parameterization.

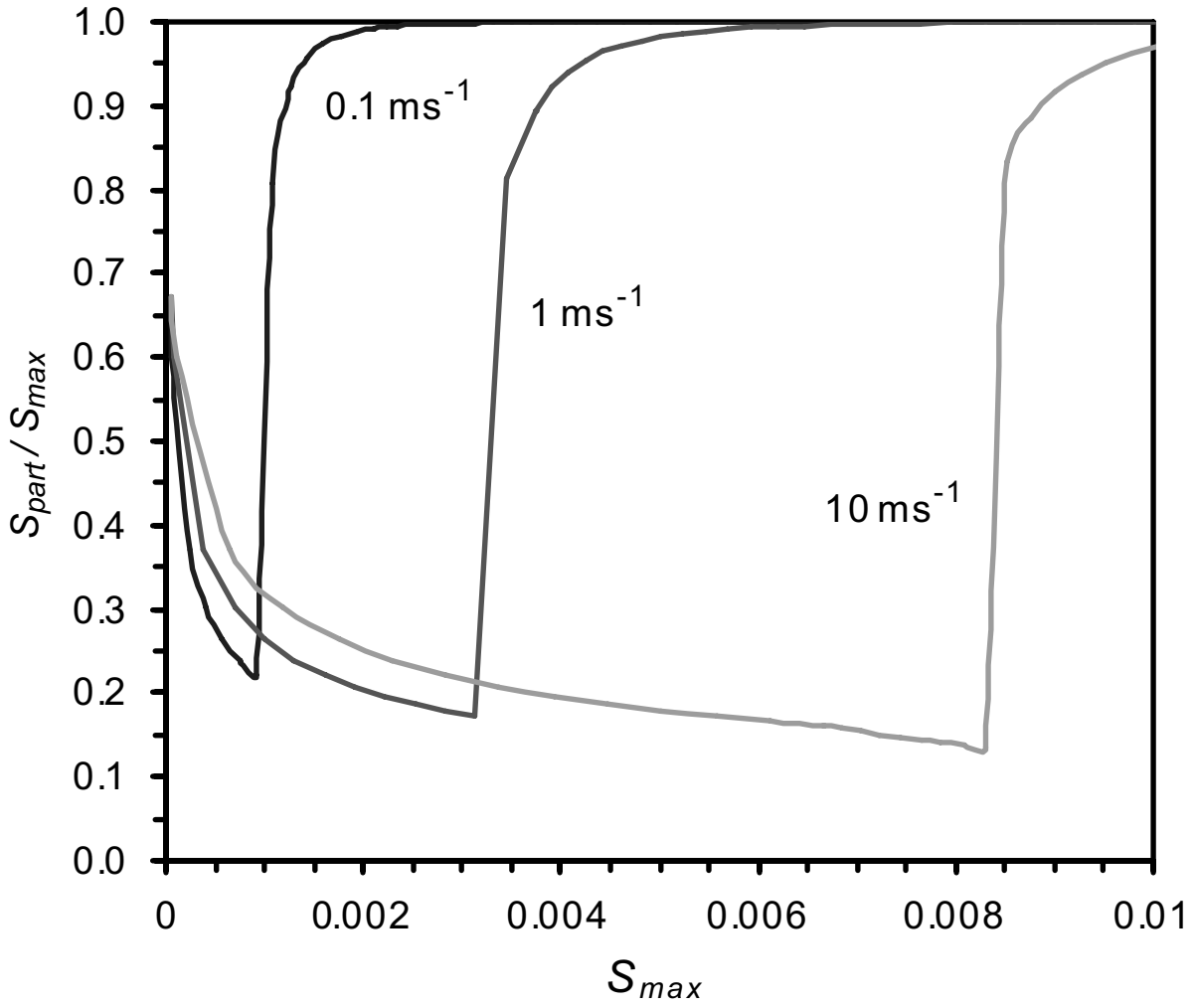

Figure 3. s_{part}/s_{max} as a function of s_{max}. Each curve corresponds to a constant updraft velocity.

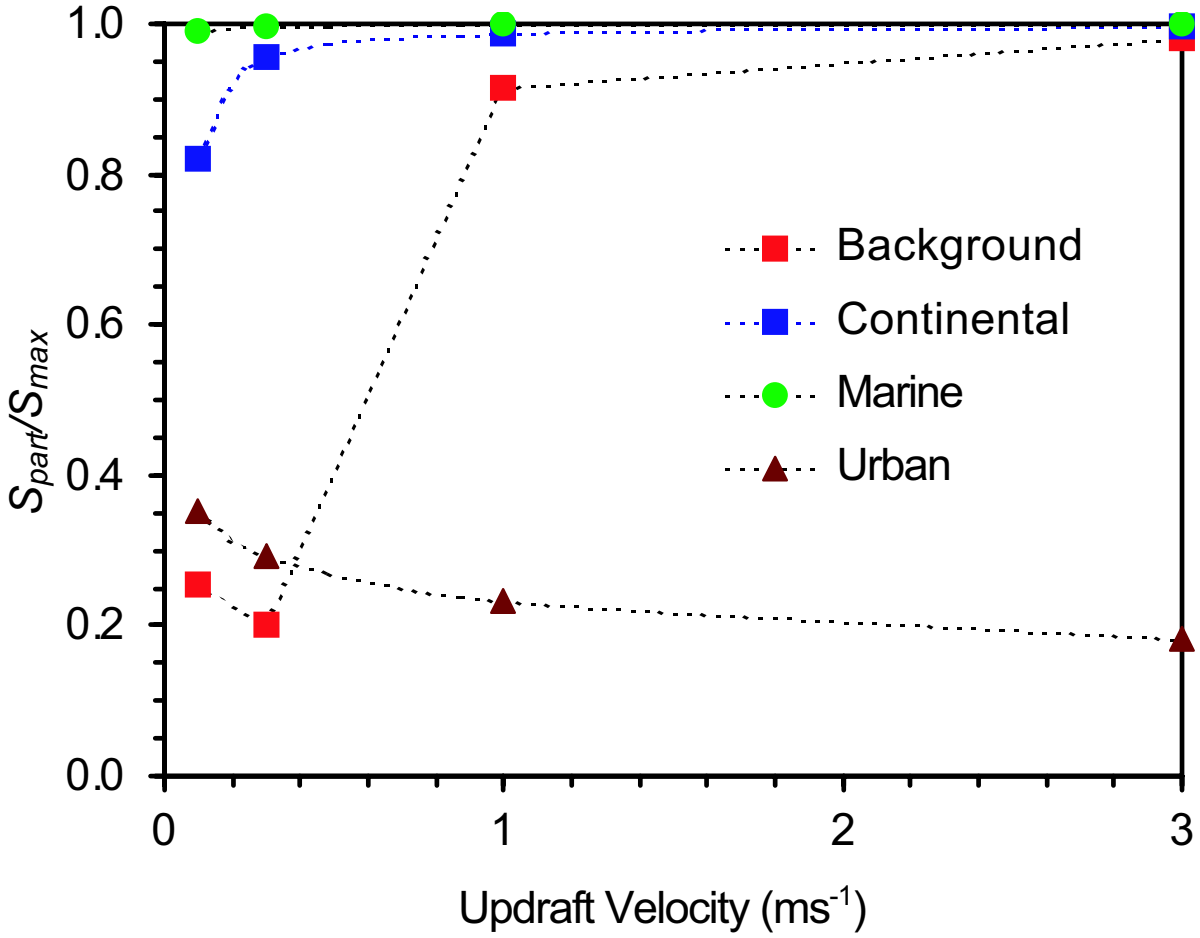

Figure 4. s_{part}/s_{max} as a function of updraft velocity. Each curve corresponds to one of the aerosol types in Table 2. s_{max} is computed using the numerical parcel model of *Nenes et al.* [2001].

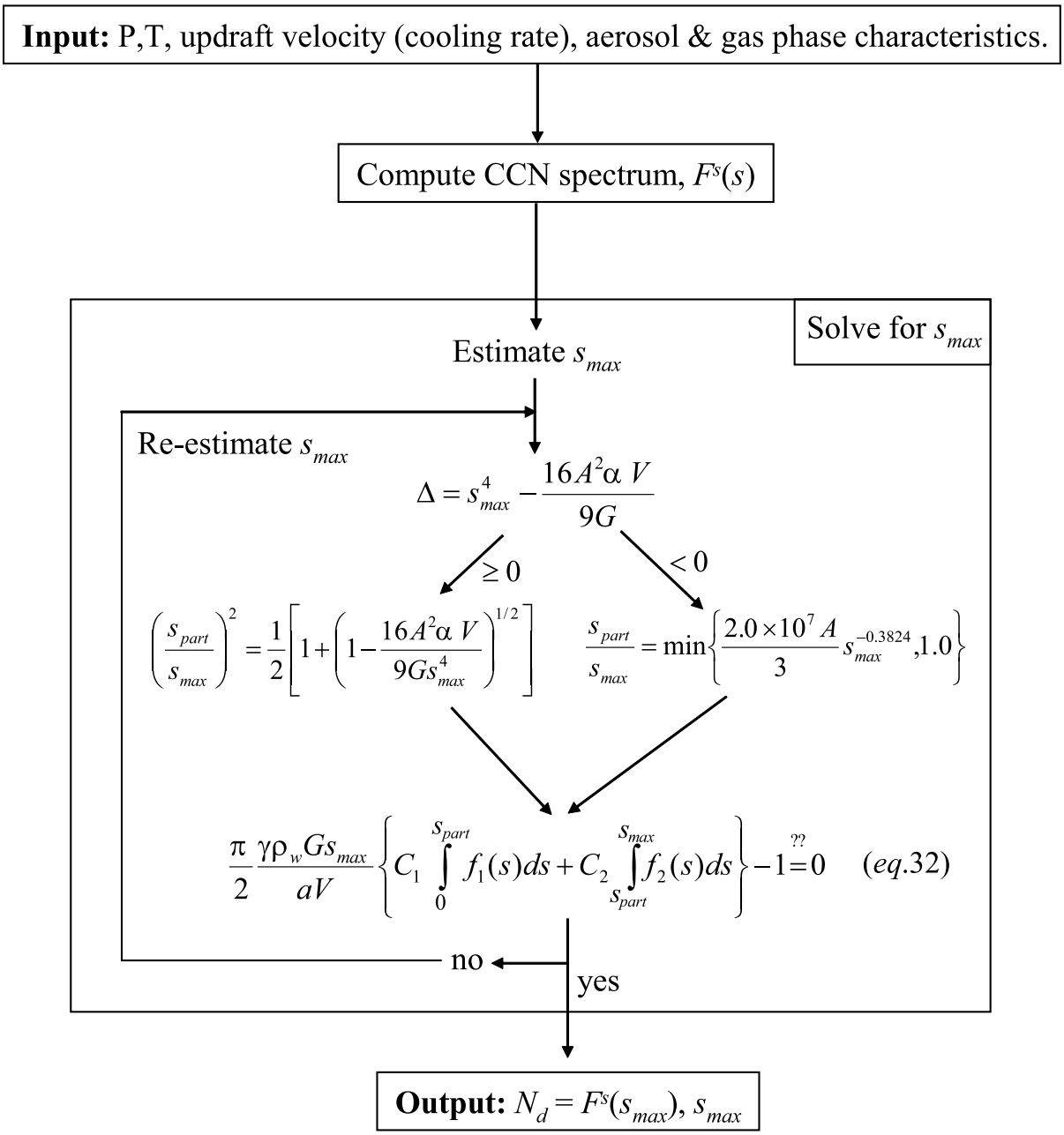

Figure 5. Parameterization algorithm.

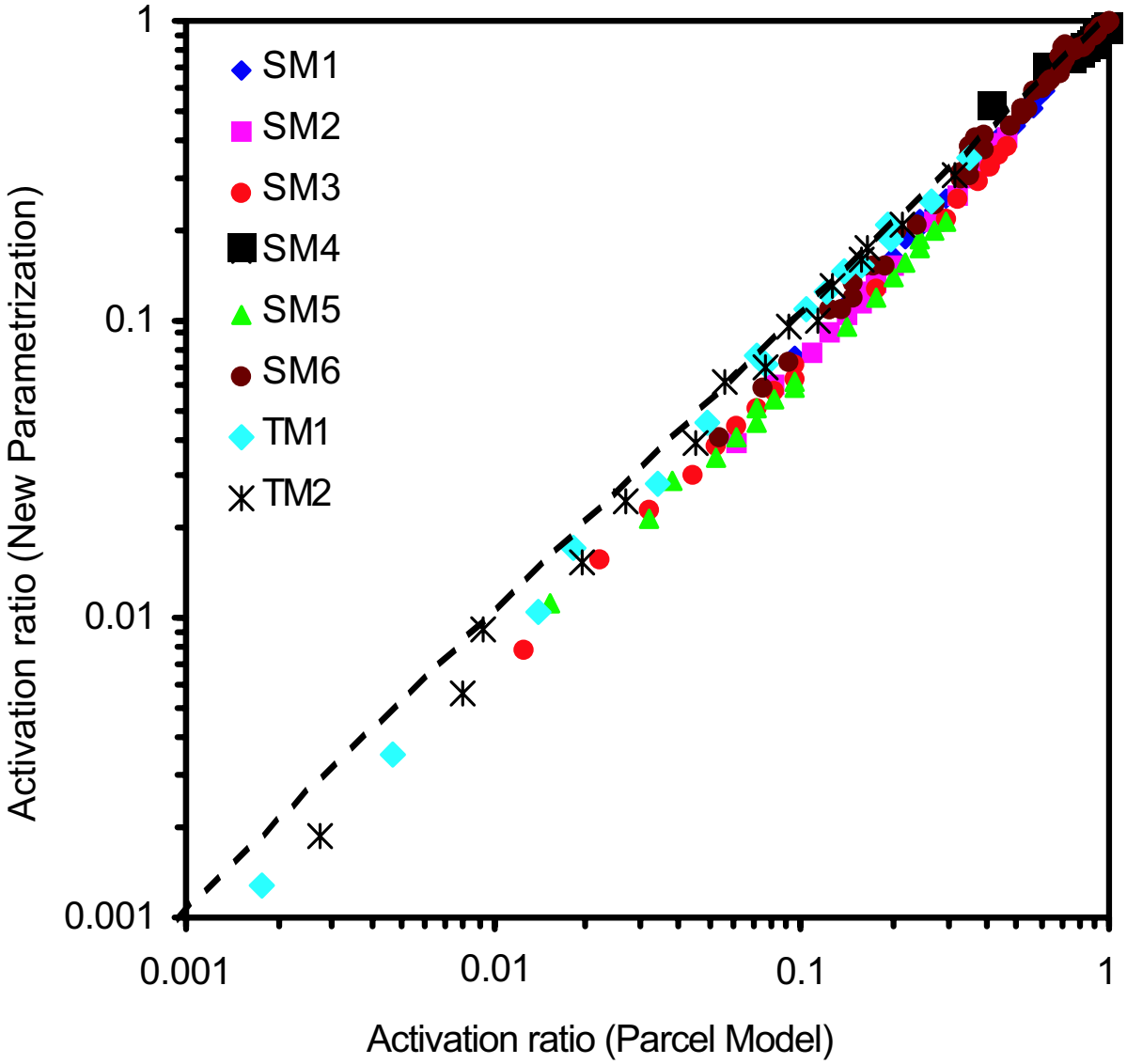

Figure 6. Fraction of aerosol that become droplets, as predicted by the new parameterization and the cloud parcel model.

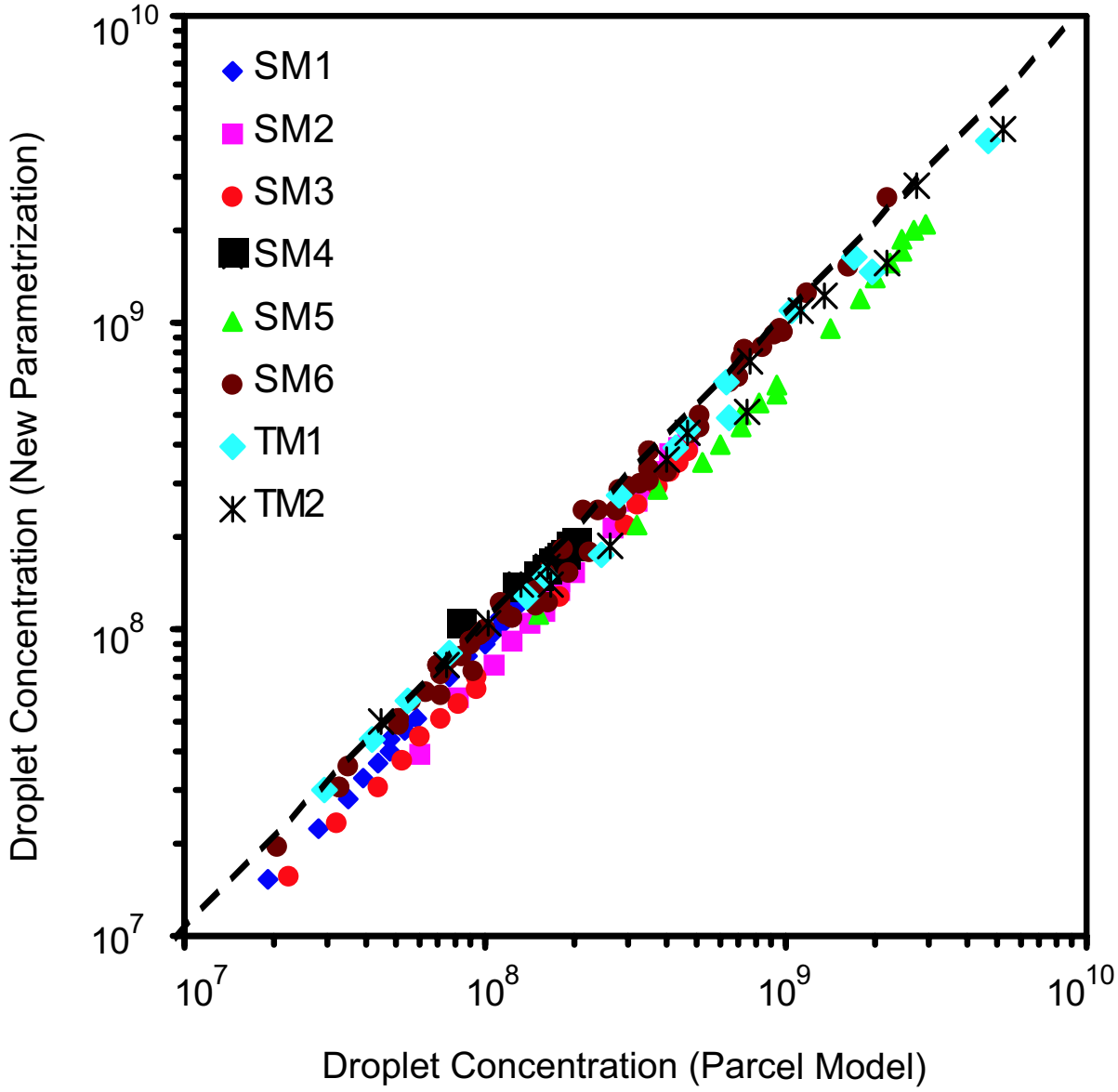

Figure 7. Droplet number concentration, as predicted by the new parameterization and the cloud parcel model.

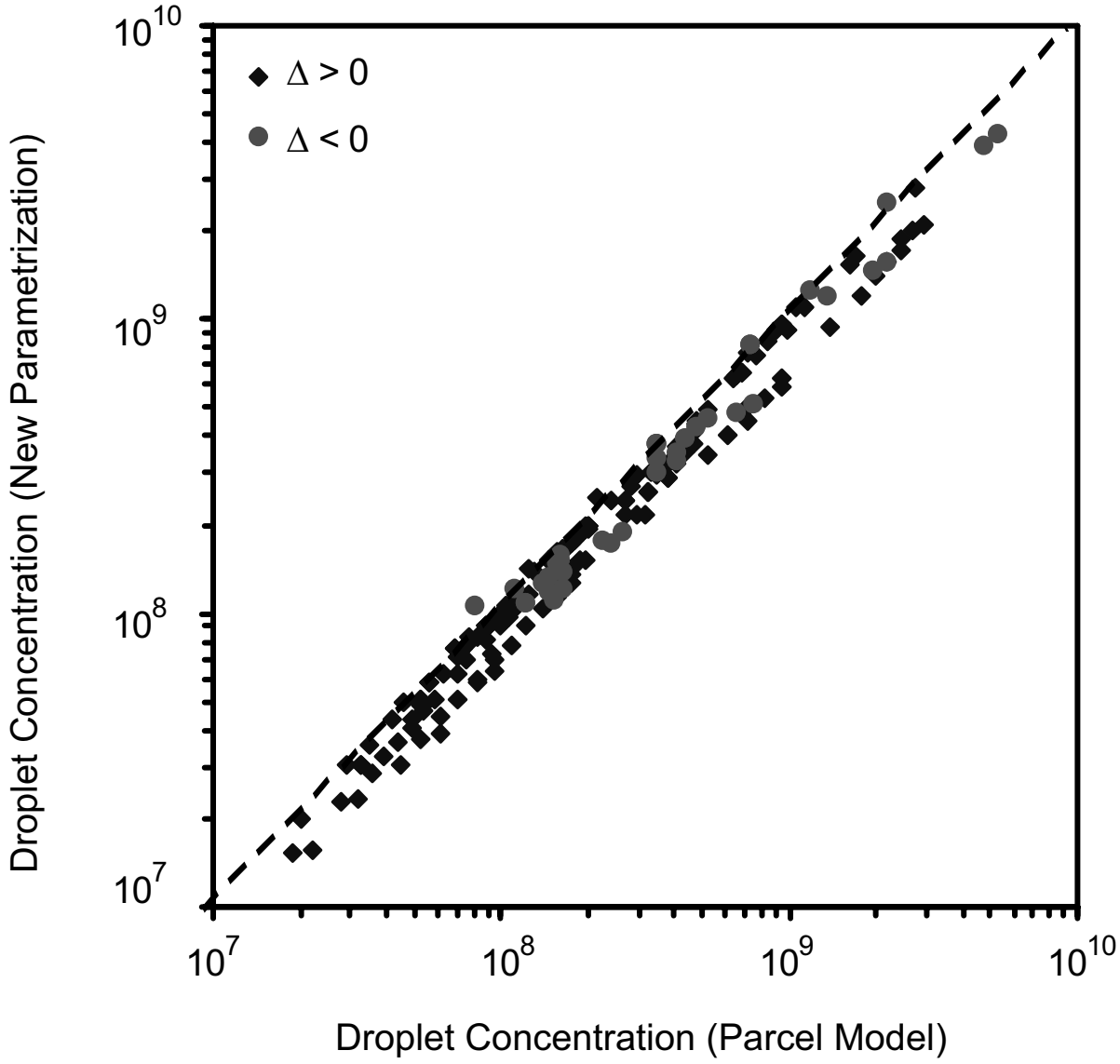

Figure 8. Droplet number concentration, as predicted by the new parameterization and the cloud parcel model. The points are colored according to the value of Δ.

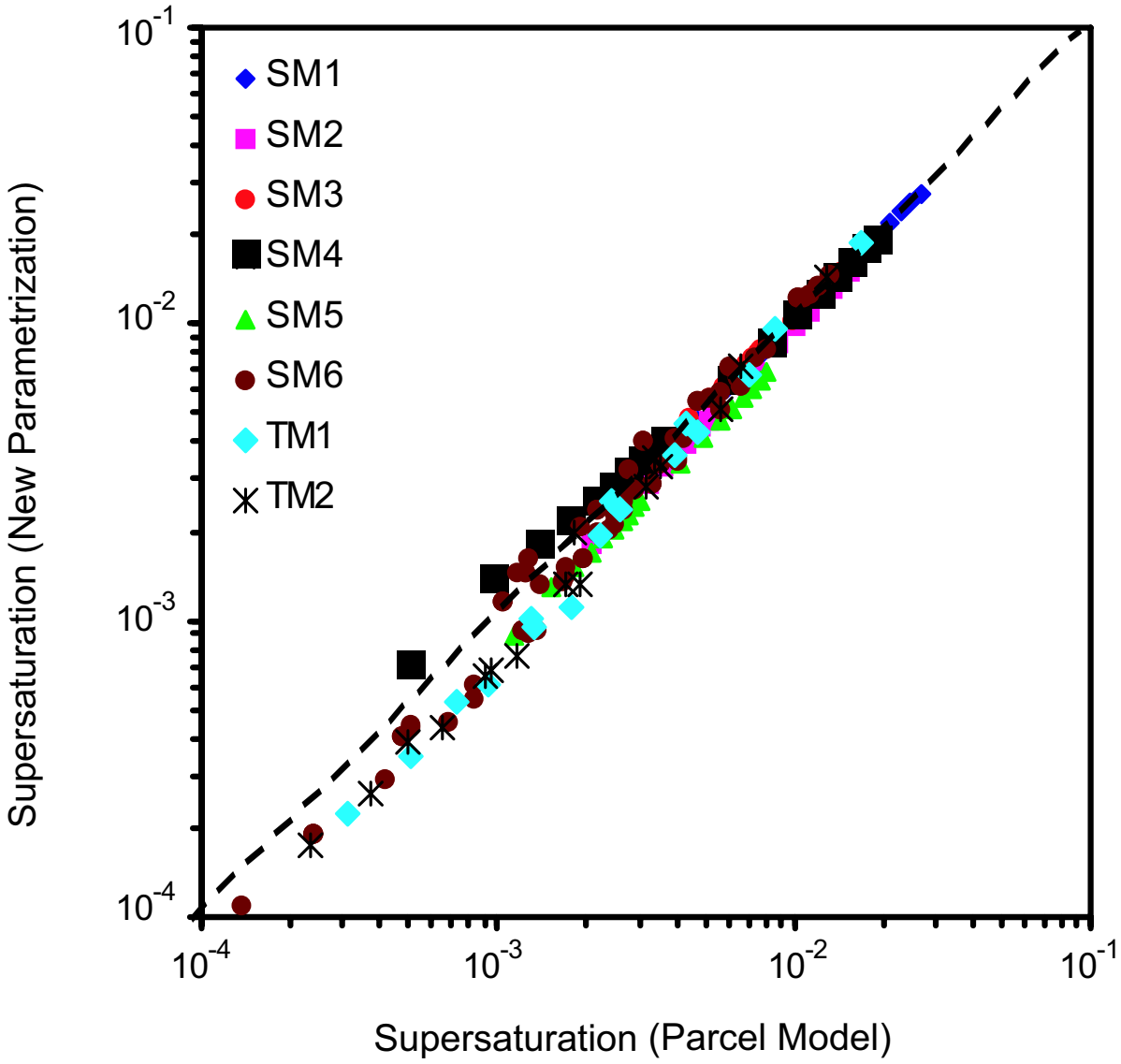

Figure 9. Maximum parcel supersaturation, as predicted by the new parameterization and the cloud parcel model.

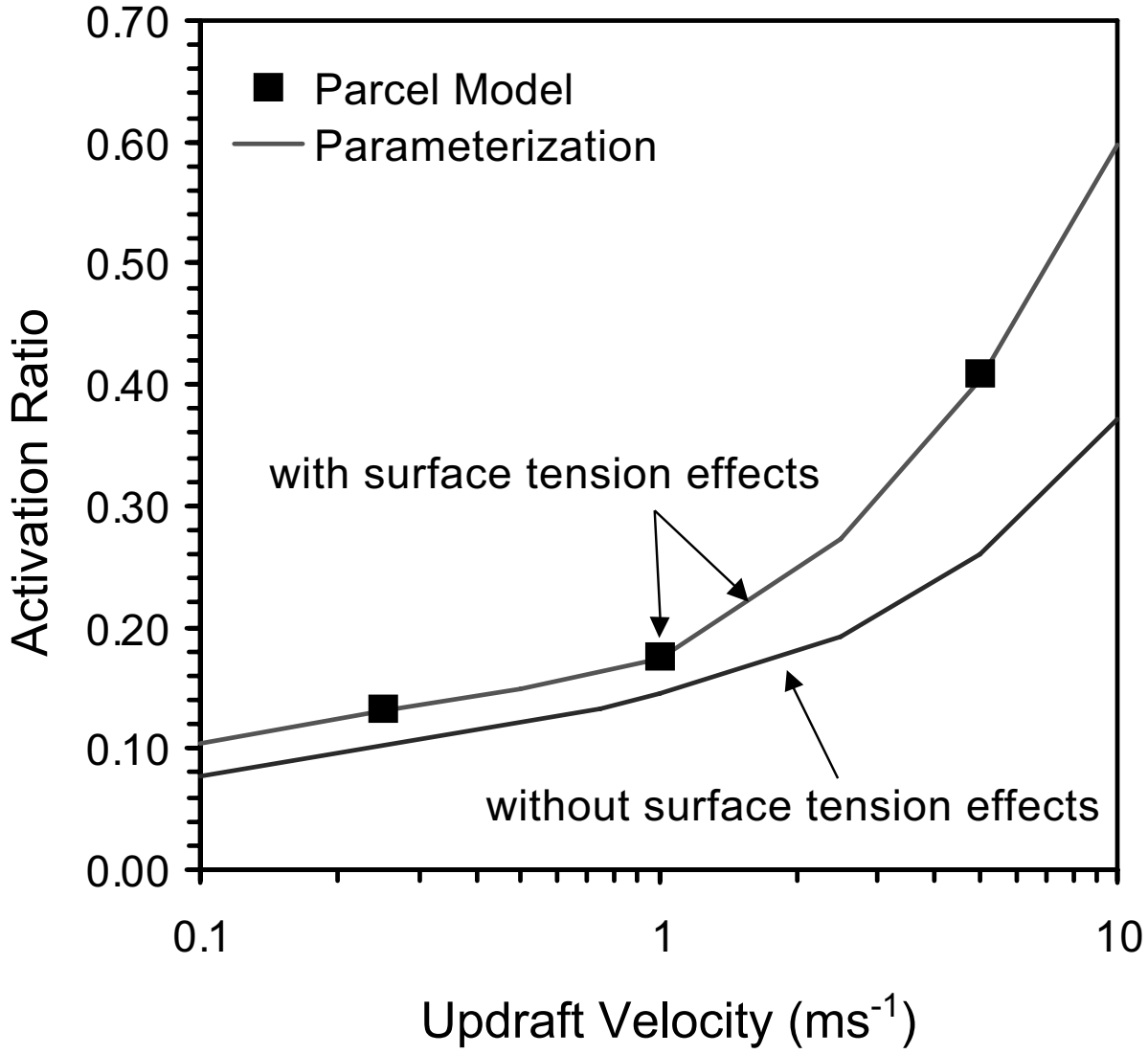

Figure 10. Activated droplet ratio, as a function of updraft velocity. Both the cloud parcel model and parameterization results (with and without the effect of the organic from changes in surface tension) are shown. The parcel model simulations include surface tension effects from the dissolved organic. Marine aerosol composed of 80% $(NH_4)_2SO_4$ and 20% organic surfactant is used. The organic surfactant behavior is described in the text.

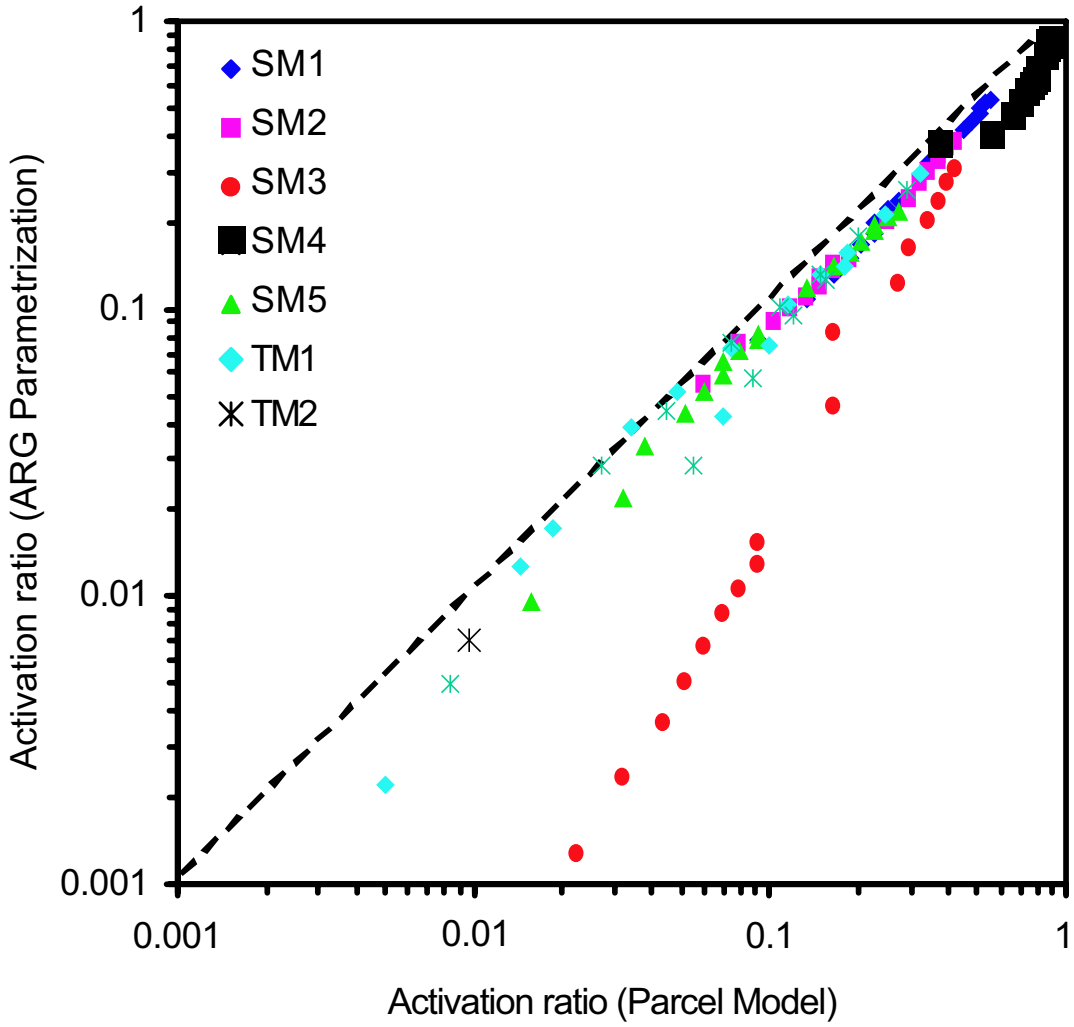

Figure 11. Fraction of aerosol that become droplets, as predicted by the *Abdul-Razzak and Ghan* [2000] parameterization and the cloud parcel model.

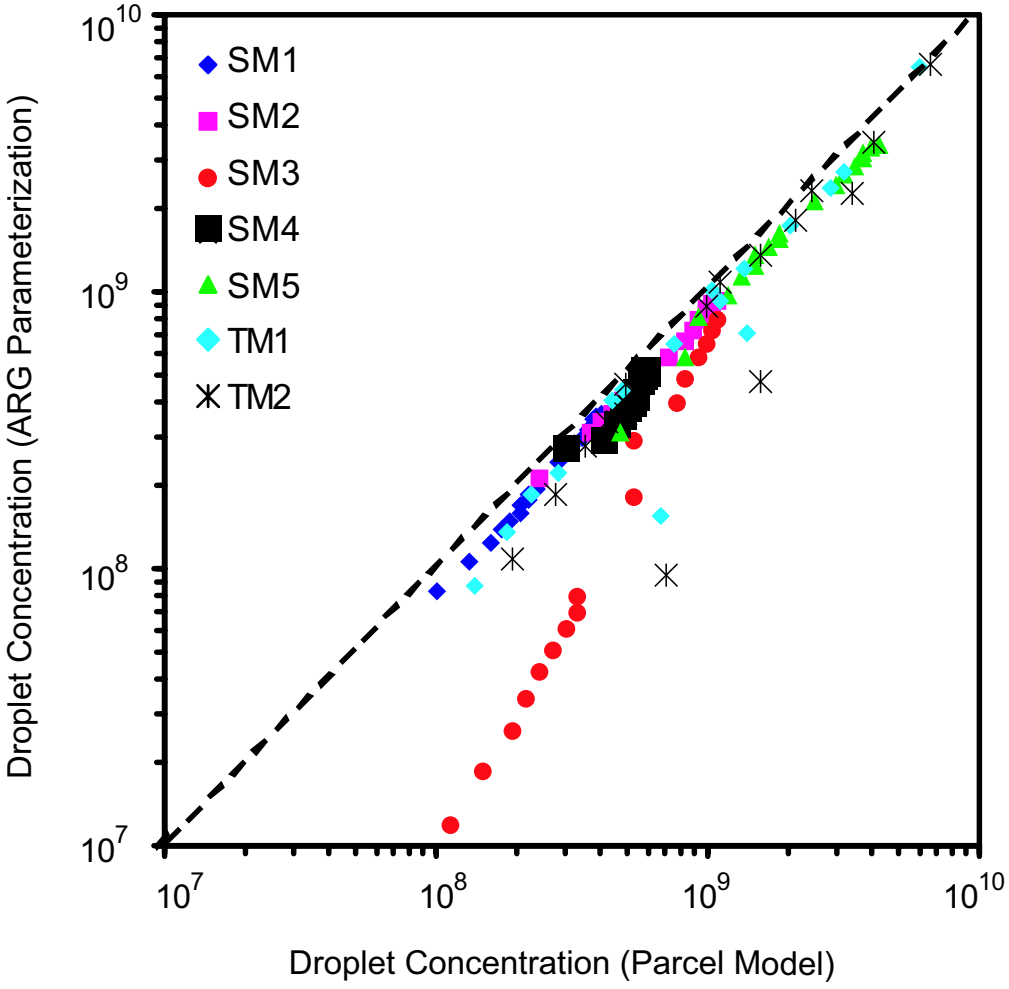

Figure 12. Droplet number concentration, as predicted by the *Abdul-Razzak and Ghan* [2000] parameterization and the cloud parcel model.